the reduction in a reporter dye color. Tissues homogenates in PBS(-) were prepared by Dounce Tissue Grinder to avoid mitochondrial damage. Tissue samples were then solubilized and diluted with detergent in the assay kit at the optimal protein concentrations for each organ to immunocapture PDH on the microplate; brain (1 mg/well), heart (200 μg/well), lungs (1 mg/well), liver (800 μg/well) and muscles (1 mg/well). After adding the reaction mixture, absorbance was monitored at 450 nm for 15 min. The activity was expressed as the initial rate of reaction.

### Western immunoblotting

Anti-mouse PDK4 antibody (provided generously by Dr. M. Horiuchi, Kagoshima University, Japan), was used for detection of PDK4 in the heart, lungs, skeletal muscles and liver tissues [27]. Freshly isolated tissues were homogenized with 7 volumes of RIPA lysis buffer containing 50 mM Tris-HCl, pH 8.0, and 150 mM NaCl, 10% glycerol, 1% NP 40, 0.5% deoxycholate, 0.4 mM EDTA, and 0.5 mM sodium orthovanadate (Thermo Scientific, Yokohama, Japan) and centrifuged at 12,000×*g* for 20 min. The extracts (with protein concentration of 16.7 μg) were used for immunoblotting, as described previously [13]. Immunoreactive bands were visualized by enhanced chemiluminescence detection system (GE Healthcare, Tokyo) and the detected bands were quantified by ImageJ software.

### Real-time PCR

Total RNA was extracted from mice tissues with RNeasy Mini kit (Qiagen, Hilden, Germany) and reverse transcribed using oligo primers and universal primers in SuperScript III RT kit (Gibco BRL, Grand Island, NY) for cDNA synthesis. RT-PCR and quantification of gene expression by real-time PCR were performed using a Fast Start Universal SYBR Green Master (Roche Diagnostics, Mannheim, Germany) on an ABI Prism 7300 system. The primer pairs used to amplify influenza A virus NS1, PDK1–4, PDP 1–2, trypsin and mouse glyceraldehyde-3-phosphate dehydrogenase (GAPDH) are listed in Table 1. PCR was initiated at 95°C for 10 min to activate HotStartTaq DNA polymerase, followed by 40 cycles of 30-s denaturation at 95°C, 30-s annealing at 52°C and 50-s extension at 72°C.

### Enzyme-linked immunosorbent assay (ELISA)

The lung samples were crushed with 3 mL PBS and IL-6, IL-2, TNF-α, IL-1β, and IFN-γ levels in the homogenates were measured using Quantikine ELISA kit (R&D systems, Minneapolis, MN). IFN-α and IFN-β levels were measured using VeriKine ELISA kits (R&D systems) according to the respective protocols provided by the manufacturer.

### Histological evaluation

After euthanasia, the lungs were isolated then fixed with 4% paraformaldehyde, dehydrated, infiltrated, and cut into 5-μm paraffin-embedded tissue sections for histological evaluation, as described previously [13]. Tissue sections were stained with hematoxylin–eosin.

### Statistical analysis

Results are presented as mean ± SD. Differences between groups were analyzed by one-way analysis of variance (ANOVA) with Tukey post hoc test. Survival rate was analyzed by the Kaplan-Meier and log-rank tests. Changes in body weight among groups were analyzed by two-way ANOVA. All statistical tests were performed using the Microsoft Excel software (Microsoft Corp, Redmond, WA) add-in Ekuseru-Toukei 2010 version 1.10 (Social Survey Research Information Co.). All *P* values are two-sided, and those less than 0.05 were considered statistically significant.

## Results

### Low PDH activity and ATP levels in various organs of mice infected with sub-lethal doses of IAV infection

Intranasal administration of 60 pfu of IAV PR/8/34(H1N1) in 15 μL of saline in 4-week-old B6 mice was semi-lethal by day 14 post-infection; the animals began to die after day 7 post-infection. Furthermore, 120 pfu was sub-lethal with 3–5% survival rate. Animals administered 200 pfu began to die after day 7 post-infection and all were dead (100% mortality rate) by day 10 (lethal dose). At day 4 post-infection and thereafter, the majority of animals infected with these doses of IAV developed clinical signs of infection (e.g., inactivity, loss of body weight, ruffled fur, labored respiration and huddling behavior). MOF starts at day 4 post-IAV-infection, and is characterized by marked increase in the levels of proinflammatory cytokines and a rapid increase in viral proliferation via the influenza virus–cytokine–trypsin cycle [7,12]. After peak viral proliferation in the lung at days 4 to 5 post-infection, various metabolic disorders associated with cellular dysfunction become obvious in various organs, together with the initiation of host protective immunity [12].

Mice infected with 120 pfu of IAV had significantly low PDH activity in the lungs at day 3 post-infection (to about 50–60% of the non-infected control) and also in the skeletal muscles, liver and

**Table 1.** Sequences of primers used in real-time PCR.

| Gene | Forward primer (5′-3′) | Reverse primer (5′-3′) |
|---|---|---|
| PDP1 | CGGGCACTGCTACCTATAATT | ACAATTTGGACGCCTCCTTACT |
| PDP2 | GGCTGAGCATTGAAGAAGCATT | GCCTGGATTTCTAGCGAGATGT |
| PDK1 | CCGGGCCAGGTGGACTTC | GCAATCTTGTCGCAGAAACATAAA |
| PDK2 | GCTTCCCCTGACCTGGAGAT | AGGCTGGACTCGGCTTT |
| PDK3 | CGGTCCCCAAGCAGATCGA | GTTAGCCAGTCGCACAGGAG |
| PDK4 | CACATGCTCTTCGAACTCTTCAAG | TGATTGTAAGGTCTTCTTTCCCAAG |
| Trypsin | AGTGGGTGGTGTCTGCAGCTCA | GATTCCTGCCAGGGTGACTC |
| NS-1 | TACCTGCGTCGCGTTACCTAA | TGCTTCTCCAAGCGAATCTCT |
| GAPDH | CATCACCATCTTCCAGGA | GAGGGGGCCATCCACAGTCTTC |

doi:10.1371/journal.pone.0098032.t001

heart at day 7 post-infection (Figure 1A). On the other hand, PDH activity in the brain remained unchanged at days 3 and 7 post-infection. ATP levels in the heart, lungs, skeletal muscles and liver, but not in the brain, showed similar reduction patterns (both time course and tendency, Figure 1B). These findings indicate that sub-lethal doses of IAV induce significant disorder of glucose oxidation, reduction of energy metabolism, and poor ATP generation in the skeletal muscles, liver, lungs and heart, through reduction of PDH activity in the mitochondria.

## IAV infection induces marked and selective up-regulation of PDK4 in the skeletal muscles, heart, lungs and liver

Oxidative decarboxylation of pyruvate involves three structurally complex enzymes, including PDH (E1), E2, and E3, that catalyze the conversion of pyruvate to acetyl-CoA [17,18]. The complex also contains two specific phosphorylation-dephosphorylation enzymes; PDK and PDP. Table 2 shows changes in relative mRNA expression levels of these regulatory compounds in the liver, heart, lungs, skeletal muscles and brain at days 0, 3 and 7 post-infection. Although a sub-lethal dose of IAV infection was associated with variable changes in the expression of these phosphorylation-dephosphorylation enzymes, marked and predominant up-regulation of PDK4 was evident in the skeletal muscles, liver, lungs and heart. However, up-regulation of PDK4 in the brain was very mild even at day 7 post-infection. Western immunoblotting analysis (Figure 2) confirmed predominant up-regulation of PDK4 protein with a peak at day 3 post-infection in the lungs, and peaks at day 7 post-infection in the skeletal muscles, heart and liver. Changes in protein levels in these organs were almost identical to those in mRNA levels.

## DADA as a novel PDK4 inhibitor

A sub-lethal dose of IAV up-regulates PDKs, particularly PDK4, resulting in the suppression of PDH activity in the mitochondria (Table 2, Figures 1 and 2). Among the known synthetic inhibitors of PDK [28], such as dichloroacetate (DCA), AZD7545 and radicicol, the pyruvate analog DCA is the most common classic inhibitor for PDK isoforms [29]. In the present study, we analyzed the inhibitory activity of DADA, a DCA derivative and commercially-available safe compound, against PDK4 and PDK2, which are the main PDK isoforms in the skeletal muscles, heart, lungs and liver [20], and used DCA as a positive control in these experiments (Table 3). Kinetic studies showed that the $IC_{50}$ values, i.e., DADA concentrations at which the reaction rates are suppressed by 50%, were 50.9 μM against PDK4 and 636.0 μM against PDK2. These values were almost identical to those of DCA against PDK4 and PDK2, respectively. These results indicate that DADA is a novel PDK4 inhibitor with about 12.5-fold higher affinity than that against PDK2.

## DADA significantly increases PDH activity and ATP levels in the skeletal muscles, heart, lungs and liver

To analyze the effects of DADA as a PDK4 inhibitor on PDH activity and ATP levels in different tissues, mice infected with a sub-lethal dose of IAV PR/8/34(H1N1) were treated orally with DADA immediately after the infection, at 50 mg/kg twice daily. As described above, the infection resulted in marked suppression of PDH activities and ATP levels at day 7 post-infection, the time point before animal death, in the skeletal muscles, liver, lungs and heart to about 25–52% and 48–63% of the non-infected control, respectively (Figure 3). DADA significantly prevented the effects of

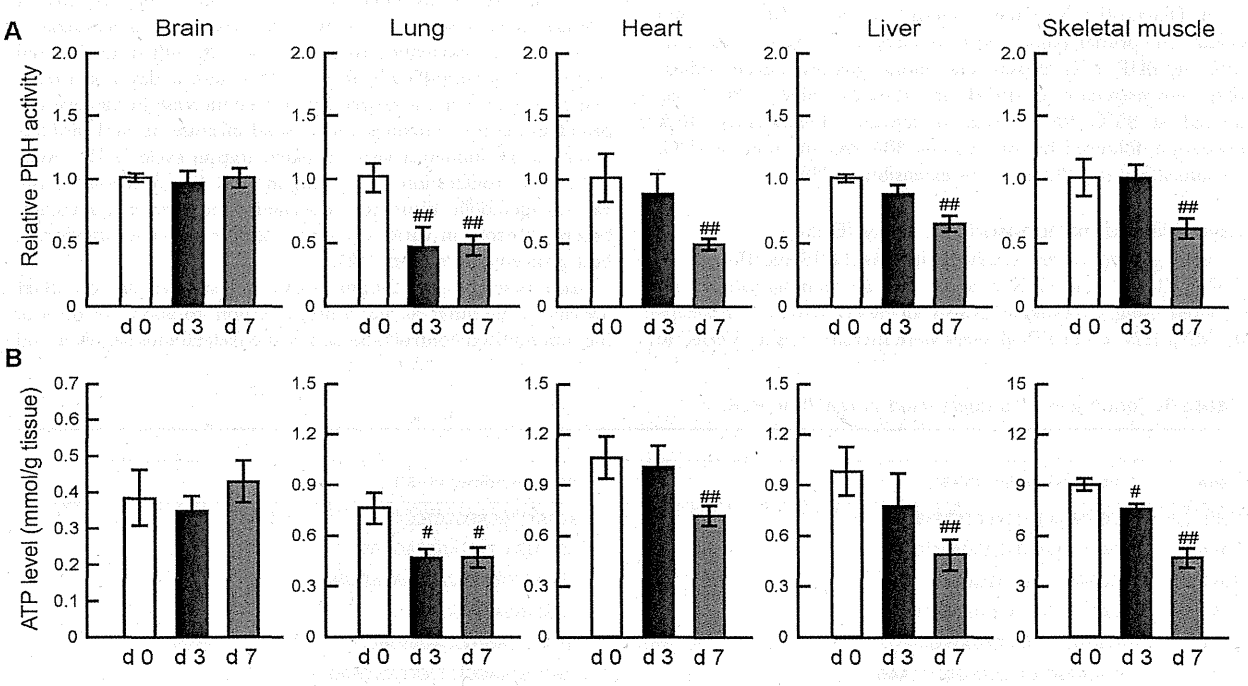


**Figure 1. Time course of changes in PDH activity and ATP levels in the skeletal muscles, heart, lungs, liver and brain of IAV-infected mice.** Mice were infected with IAV/PR/8/34(H1N1) at 120 pfu intranasally and the levels of PDH activity (A) and ATP (B) in the skeletal muscles, heart, lungs, liver and brain were analyzed at days 0 (d0), 3 (d3) and 7 (d7) post-infection. PDH activity levels after IAV infection relative to the values at day 0. Data are mean ± SD of 5 mice per group. $^{\#}P<0.05$, $^{\#\#}P<0.01$ vs. day 0, by one-way analysis of variance (ANOVA) with Tukey post hoc test.
doi:10.1371/journal.pone.0098032.g001

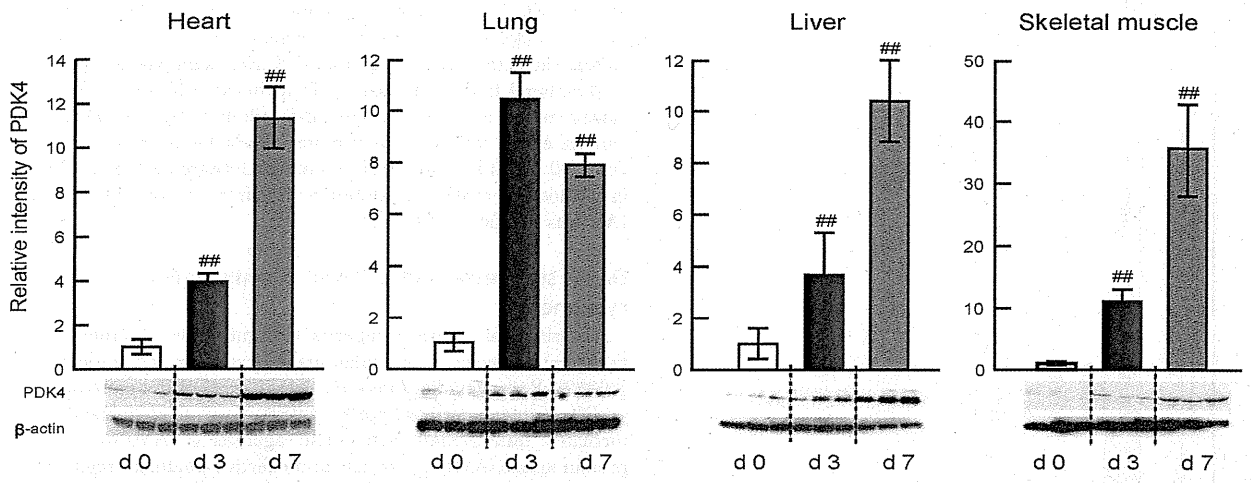


**Figure 2. Time course of changes in PDK4 protein expression levels in the skeletal muscles, heart, lungs and liver of IAV-infected mice.** Mice were infected with 120 pfu of IAV, and PDK4 protein expression levels in the skeletal muscles, heart, lungs and liver were measured by western immunoblotting at day 0 (d0), day 3 (d3) and day 7 (d7) post-infection. β-Actin was used as internal control. PDK4 expression levels after IAV infection relative to the values at day 0. Data are mean ± SD of three experiments from 5 mice per band. *$P<0.05$, **$P<0.01$, vs. day 0, by one-way analysis of variance (ANOVA) with Tukey post hoc test.
doi:10.1371/journal.pone.0098032.g002

IAV infection and restored PDH activities to levels similar to those recorded before infection. DADA also increased ATP levels to 68–130% of non-infected control in the skeletal muscles, heart, lungs and liver. On the other hand, PDH activity and ATP levels in the brain were neither affected by the infection nor DADA treatment.

## DADA tends to normalize biased blood glucose, lactate, β-hydroxybutyric acid, free fatty acids, and ATP levels after infection

Since PDH activity is closely linked to homeostasis of glucose, lipid, ketones, lactate and ATP [17–20], we next measured blood glucose, lactate, β-hydroxybutyric acid, free fatty acids and ATP levels at day 7 post-infection in untreated and DADA-treated mice

**Table 2.** Relative mRNA expression levels of PDPs and PDKs after severe IAV infection.

| | Days after infection | Brain | Heart | Lung | Liver | Skeletal muscle |
|---|---|---|---|---|---|---|
| PDP1 | Day 0 | 1.0±0.31 | 1.0±0.18 | 1.0±0.23 | 1.0±0.12 | 1.0±0.06 |
| | Day 3 | 1.20±0.43 | 0.88±0.42 | 1.21±0.13 | 2.30±0.42$^{\#\#}$ | 0.72±0.21 |
| | Day 7 | 0.68±0.24 | 0.66±0.20 | 0.43±0.11 | 2.77±0.22$^{\#\#}$ | 0.30±0.09$^{\#\#}$ |
| PDP2 | Day 0 | 1.0±0.37 | 1.0±0.12 | 1.0±0.12 | 1.0±0.18 | 1.0±0.18 |
| | Day 3 | 2.0±0.52$^{\#}$ | 0.26±0.05$^{\#\#}$ | 1.51±0.56 | 2.19±0.24$^{\#}$ | 1.12±0.10 |
| | Day 7 | 2.2±0.31$^{\#}$ | 0.20±0.06$^{\#\#}$ | 0.76±0.09 | 1.78±0.31$^{\#}$ | 2.17±0.27$^{\#\#}$ |
| PDK1 | Day 0 | 1.0±0.06 | 1.0±0.27 | 1.0±0.21 | 1.0±0.13 | 1.0±0.09 |
| | Day 3 | 1.25±0.40 | 0.87±0.21 | 0.69±0.17 | 0.85±0.49 | 0.82±0.21 |
| | Day 7 | 1.38±0.34 | 0.81±0.18 | 0.69±0.21 | 0.98±0.43 | 0.60±0.12$^{\#}$ |
| PDK2 | Day 0 | 1.0±0.06 | 1.0±0.18 | 1.0±0.23 | 1.0±0.12 | 1.0±0.18 |
| | Day 3 | 1.56±0.34 | 0.93±0.43 | 0.40±0.11 | 2.05±0.37$^{\#}$ | 1.12±0.12 |
| | Day 7 | 1.76±0.21 | 1.25±0.61 | 0.15±0.04 | 1.25±0.14 | 1.18±0.20 |
| PDK3 | Day 0 | 1.0±0.37 | 1.0±0.06 | 1.0±0.08 | 1.0±0.18 | 1.0±0.12 |
| | Day 3 | 1.23±0.34 | 1.02±0.24 | 1.16±0.43 | 3.55±0.49$^{\#\#}$ | 0.68±0.18 |
| | Day 7 | 1.01±0.24 | 1.07±0.15 | 1.01±0.09 | 4.68±0.31$^{\#\#}$ | 0.75±0.20 |
| PDK4 | Day 0 | 1.0±0.06 | 1.0±0.07 | 1.0±0.15 | 1.0±0.37 | 1.0±0.34 |
| | Day 3 | 1.26±0.21 | 6.57±1.34$^{\#\#}$ | 5.01±1.23$^{\#\#}$ | 1.94±0.11 | 12.46±5.46$^{\#\#}$ |
| | Day 7 | 1.37±0.1$^{\#}$ | 11.59±0.24$^{\#\#}$ | 3.59±1.34$^{\#\#}$ | 7.97±1.60$^{\#\#}$ | 85.32±7.99$^{\#\#}$ |

Data are mean ± SD.
$^{\#}P<0.05$,
$^{\#\#}P<0.01$, vs. before infection (Day 0) for each organ, by one-way analysis of variance and Turkey post hoc test.
doi:10.1371/journal.pone.0098032.t002

**Table 3.** DCA- and DADA-induced percent inhibition and related $IC_{50}$ values (μM).

| | | DCA | | | DADA | | |
|---|---|---|---|---|---|---|---|
| | | 100 μM | 300 μM | 1000 μM | 100 μM | 300 μM | 1000 μM |
| % inhibition | PDK2 | 9.0±0.3 | 33.0±0.18 | 58.4±3.3 | 16.6±0.2 | 37.8±0.2 | 57.2±4.1 |
| | PDK4 | 63.9±3.3 | 88.0±1.0 | 97.8±12 | 70.2±2.1 | 93.4±10 | 99.1±13 |
| $IC_{50}$ (μM) | PDK2 | | 676.0 | | | 636.0 | |
| | PDK4 | | 57.8 | | | 50.9 | |

Data are mean ± SD.

doi:10.1371/journal.pone.0098032.t003

infected with 120 pfu and 200 pfu of IAV (Figure 4). Mice infected with both doses of IAV showed decrease in glucose levels and increase in lactate, free fatty acids and β-hydroxybutyric acid levels in peripheral blood, with slight fall in blood ATP levels. These values tended to normalize after oral administration of DADA, and the effects of DADA were more remarkable in mice infected with 200 pfu of IAV than 120 pfu of IAV. Restoration by DADA in all blood metabolites analyzed in mice infected with 200 pfu of IAV was significant ($P<0.01$).

## DADA suppresses induction of proinflammatory cytokines

Experimental evidence suggests that metabolic disorders are tightly interconnected with inflammatory cytokines and adipokines [30–32]. Recent studies indicated that agonists of the peroxisome proliferation-activated receptor (PPAR)-γ, a lipid metabolite-mediated transcription factor, and agonists of AMP-activated protein kinase (AMPK), are safe and effective treatment regimens in patients with diabetes mellitus, significantly mitigate the IAV-induced immunopathology with cytokine storm as immunomodulatory agents, and protect mice against lethal IAV infection [33,34]. These findings suggest that metabolic disorders induced by IAV infection are interconnected with cytokine up-regulation probably through metabolite-mediated signaling pathways and transcription factors.

Next, we assessed the effects of DADA treatment on cytokine levels at day 2 post-infection during cytokine storm duration in the lungs of mice [12,35] infected with a sub-lethal dose of IAV. IAV infection significantly increased the levels of all tested proinflammatory cytokines (IL-1β, IL-6, IL-2, TNF-α, IFN-α, IFN-β and IFN-γ) in lung homogenates between 1.2- and 13.7-fold relative to the baseline (before infection) (Figure 5). Treatment with DADA significantly suppressed IL-6, IL-2, IFN-α, TNF-α and IFN-γ levels but not those of IFN-β and IL-1β.

## DADA reduces IAV replication in the lungs and trypsin expression in various organs

Since the levels of proinflammatory cytokines are closely interconnected to those of trypsin and influenza virus replication rate in target organs through the influenza virus–cytokine–trypsin cycle [7,12,13], we analyzed the effects of DADA on viral replication and trypsin expression in the lungs during the peak duration at days 2, 4 and 6 post-infection [7,36,37] and in other organs at day 4 post-infection [7,13,38]. Quantitative real-time PCR showed a significant reduction in the copy number of the viral non-structure protein 1 (NS-1) RNA gene segment in the lungs of infected mice treated with DADA at days 4 and 6 post-infection, compared with the vehicle-treated mice (Figure 6). Furthermore, the markedly induced trypsin levels in the lungs at day 2 post-infection and those in the skeletal muscles, heart and brain at day 4 post-infection were significantly suppressed in animals treated with DADA (Figure 7). However, IAV infection and DADA treatment had no significant effects on trypsin expression in the liver.

## DADA significantly increases survival rate of mice infected with semi- and sub-lethal doses of IAV and restores suppressed food and water intake after infection

We also studied the effects of DADA on survival rate, body weight and food and water intake of mice infected with 60 and 120 pfu of IAV during the 14-day post-infection period. Mice infected with 60 pfu of IAV showed progressive avoidance of food and water during days 2 to 7 post-infection, and the animals died

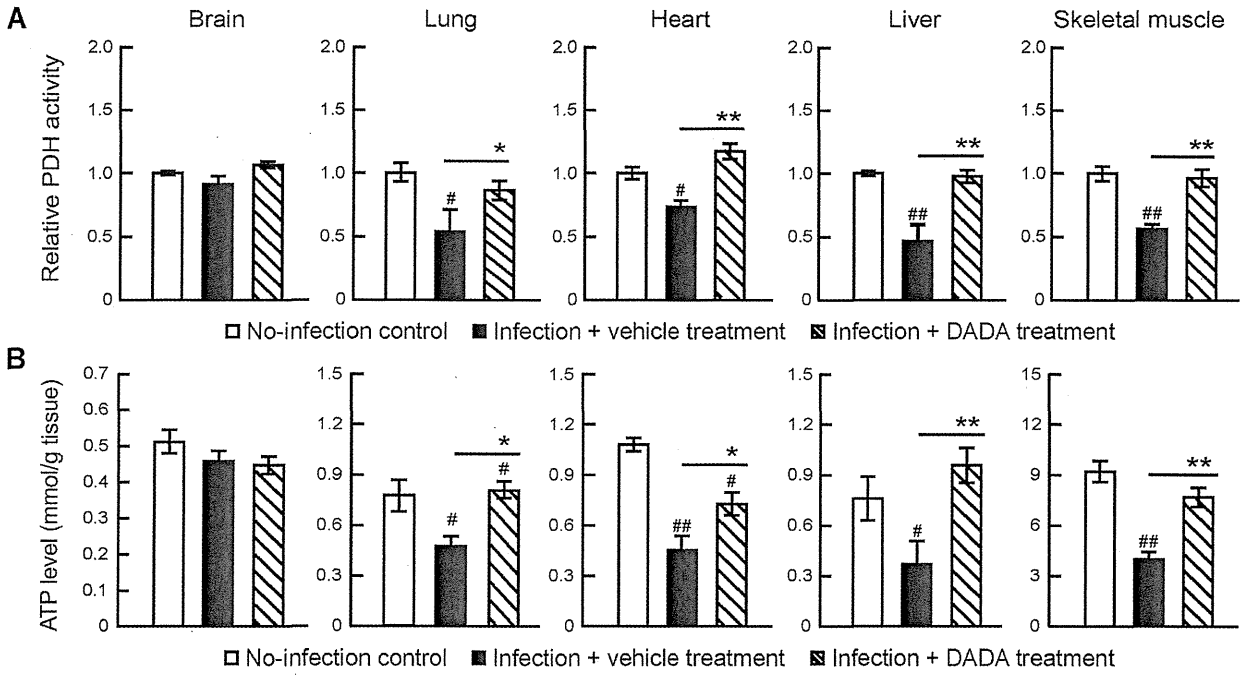


**Figure 3. Treatment with DADA restores suppressed PDH activity and ATP levels in the skeletal muscles, heart, lungs and liver of IAV-infected mice.** Mice infected with 120 pfu of IAV were treated orally with DADA at 50 mg/kg or vehicle at 12-h intervals for 14 days, and the levels of PDH activity (A) and ATP (B) in the skeletal muscles, heart, lungs, liver and brain of mice were analyzed at day 7 post-infection. PDH activity levels relative to the values of the control (no-infection). Values are mean ± SD of 5 mice per group. $^{\#}P<0.05$, $^{\#\#}P<0.01$, vs. no-infection, $^{*}P<0.05$, $^{**}P<0.01$, vs. infected group treated with vehicle, by one-way analysis of variance (ANOVA) and Tukey post hoc test.
doi:10.1371/journal.pone.0098032.g003

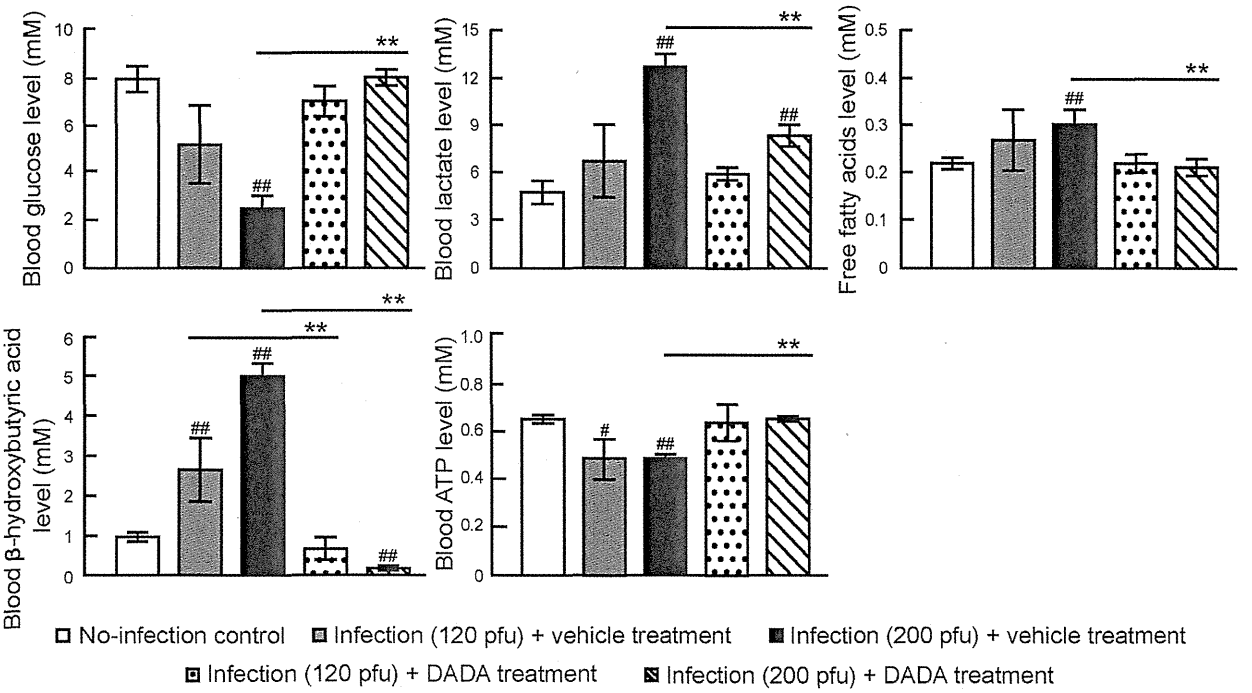


**Figure 4. DADA improves blood glucose, lactate, β-hydroxybutyric acid, free fatty acids and ATP levels.** Mice infected with 120 and 200 pfu of IAV were treated with oral DADA at 50 mg/kg or vehicle at 12-h intervals and the levels of glucose, lactate, free fatty acids, β-hydroxybutyric acid, and ATP in the blood were analyzed at day 7 post-infection. Values are mean ± SD of 5 mice per group. $^{\#}P<0.05$ and $^{\#\#}P<0.01$ vs. no-infection. $^{*}P<0.05$, $^{**}P<0.01$, vs. infected group treated with vehicle, by one-way analysis of variance (ANOVA) and Tukey post hoc test.
doi:10.1371/journal.pone.0098032.g004

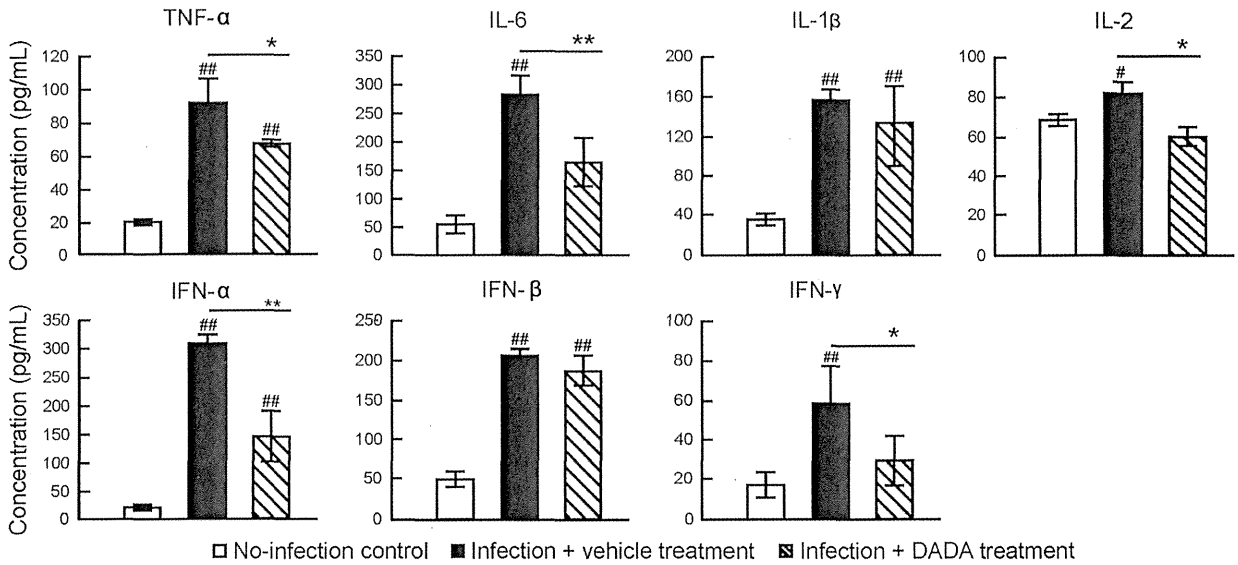


**Figure 5. DADA suppresses induction of various cytokines in the lungs of IAV-infected mice.** Mice infected with 120 pfu of IAV were treated with oral DADA at 50 mg/kg or vehicle at 12-h intervals and the levels of various cytokines in the lungs at day 2 post-infection were analyzed by ELISA. Data are mean ± SD of 5 mice per group. $^{\#}P<0.05$, $^{\#\#}P<0.01$, vs. no-infection, $^{*}P<0.05$, $^{**}P<0.01$, vs. infected group treated with vehicle, by one-way analysis of variance (ANOVA) with Tukey post hoc test.
doi:10.1371/journal.pone.0098032.g005

after infection for 7 days (Figure 8). The body weight started to fall one day after the reduction in food and water intake. However, DADA-treated infected mice showed no significant decrease in food and water intake as well as no significant reduction in body weight during the 14-day experimental period. While infected mice showed continuous decrease in the survival rate after day 7, with a survival rate of 50% at day 14 post-infection, none of the DADA-treated mice died during the experimental period. The effects of DCA administered at an equivalent molar dose to DADA, on survival rate and body weight of infected mice paralleled those of DADA during the experimental period. The time courses of avoidance of food and water of mice infected with 120 pfu of IAV were similar to those in mice infected with 60 pfu of IAV. Although mice showed continuous decrease in the survival rate after day 7 post-infection to 5% at day 14 post-infection, DADA treatment significantly reduced mortality from 95% to 50% ($P<0.05$) (data not shown).

## DADA improves pathological changes in the lungs after infection

Finally, we prepared histological sections of the lungs of mice infected with 60 pfu of IAV to confirm the effects of DADA at

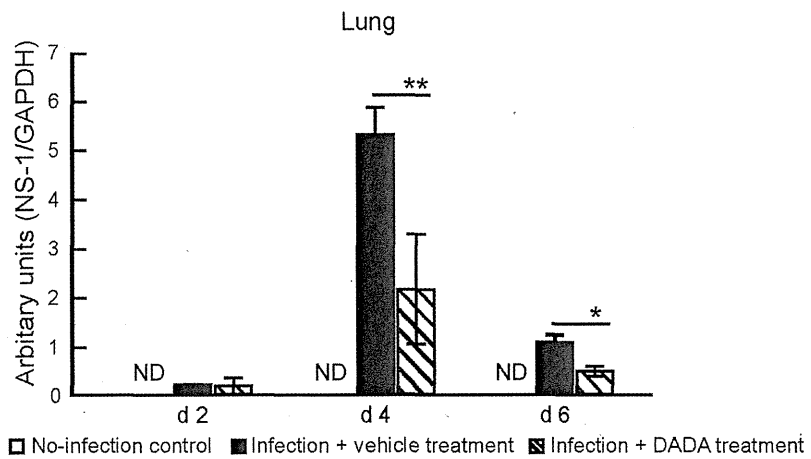


**Figure 6. Effects of DADA on viral replication.** Mice infected with 120 pfu of IAV were treated with oral DADA at 50 mg/kg or vehicle at 12-h intervals and viral NS1 replication in the lungs was analyzed quantitatively by real-time PCR at days 2 (d2), 4 (d4) and 6 (d6) post-infection. Data were normalized relative to GAPDH expression, which was used as the internal control. Open columns: control (no-infection) group [values are below the detection level (ND)]. Data are mean ± SD of three experiments in 3 mice per group. $^{*}P<0.05$, $^{**}P<0.01$, vs. infected group treated with vehicle, by one-way analysis of variance (ANOVA) and Tukey post hoc test.
doi:10.1371/journal.pone.0098032.g006

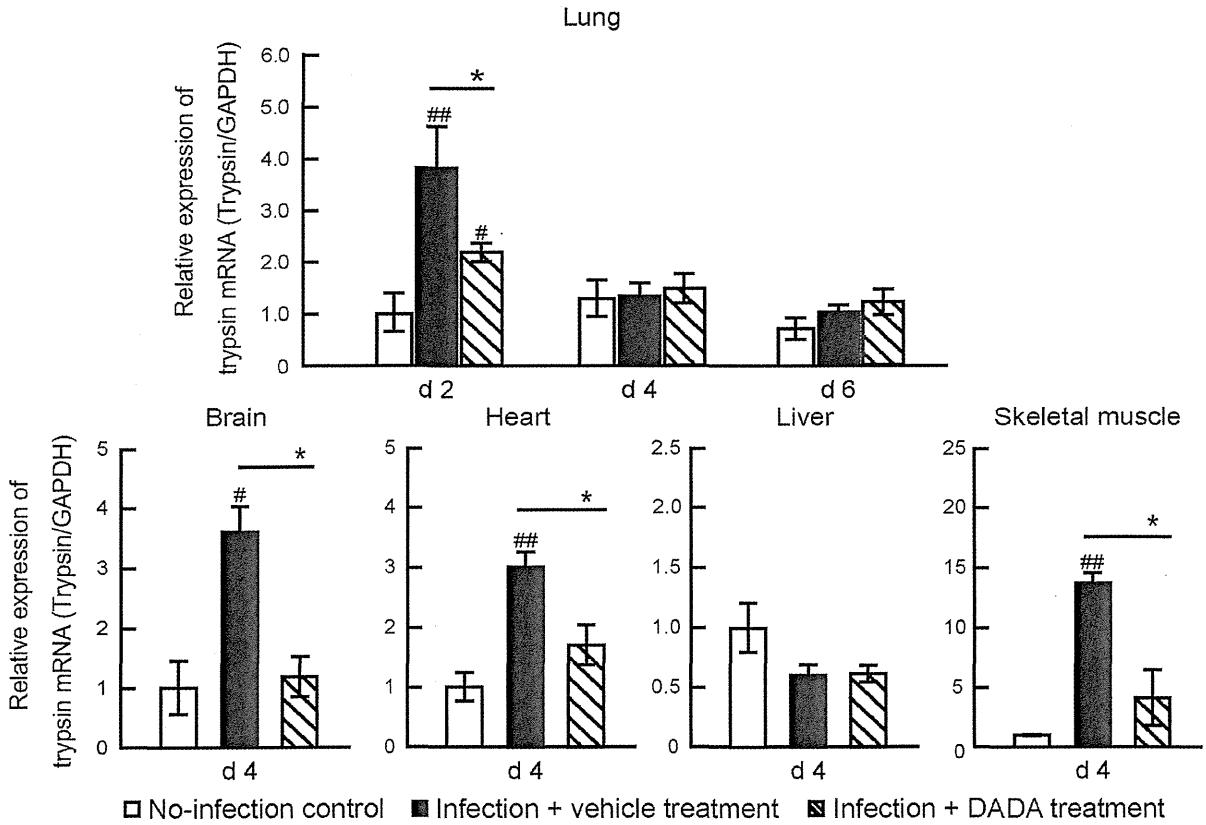


**Figure 7. Effects of DADA on trypsin up-regulation.** Mice infected with 120 pfu of IAV were treated with oral DADA at 50 mg/kg or vehicle at 12-h intervals and trypsin mRNA levels in the skeletal muscles, heart, liver and brain were measured by real-time PCR at day 4 post-infection. Trypsin mRNA levels in the lungs were also measured at days 2 (d2), 4 (d4) and 6 (d6) post-infection. Trypsin mRNA expression levels after IAV infection relative to that of no-infection. Values are mean ± SD of three experiments in 5 mice per each group. $^{\#}P<0.05$, $^{\#\#}P<0.01$, vs. no-infection, $^{*}P<0.05$, $^{**}P<0.01$, vs. infected mice treated with vehicle, by one-way analysis of variance (ANOVA) and Tukey post hoc test.
doi:10.1371/journal.pone.0098032.g007

days 0, 2, 4 and 6 post-infection using hematoxylin and eosin-stained sections of the lungs (Figure 9). In infected animals treated with vehicle, focal inflammatory infiltrates were noted in the lungs at day 2 post-infection, followed by progressive and extensive infiltration throughout the entire lungs at days 4 and 6 post-infection. DADA treatment effectively suppressed the inflammatory infiltration during days 0 and 6 post-infection, although mild infiltrates were detected at days 4 and 6 post-infection (Figure 9).

## Discussion

The present study reported several new findings: (i) Severe IAV infection markedly up-regulated PDK4, together with down-regulation of energy homeostasis and disorders of glucose and lipid metabolism. The results suggest that PDK4 is a sensitive biomarker of MOF and a target molecule for treatment in severe IAV infection. (ii) DADA effectively inhibited PDK4, with inhibition kinetics similar to DCA. (iii) DADA-induced PDK4 inhibition effectively suppressed IAV-induced MOF *in vivo*, with amelioration of suppressed energy homeostasis, disorders of glucose and lipid metabolism and cytokine up-regulation, and suppressed viral replication. The results suggest that PDK4 is a potentially suitable therapeutic target for MOF in severe IAV infection.

Until recently, most influenza virologists have concentrated on the development of therapeutic strategies that target virus replication [39]. However, MOF starts just after the peak of viral proliferation with the induction of host cellular defense system, such as innate and adaptive immune responses [12]. Furthermore, anti-viral neuraminidase inhibitors do not offer effective treatment for MOF after viral proliferation. Previous studies on the potential therapies proposed the use of various immunomodulatory agents, such as agonists of PPARγ and AMPK, with the potential of mitigating the effects of IAV-induced cytokine storm [33], although the precise mechanisms of the therapeutic actions of these agents remain so far elusive. On the other hand, studies on the pathogenesis of MOF discussed the influenza virus–cytokine–trypsin cycle as the pathomechanism of vascular hyperpermeability in MOF with cytokine storm in severe IAV infection and influenza-associated encephalopathy [5,7,13]. Upregulation of TNF-α alters the cellular redox state through its receptor and reduces ATP synthesis in mitochondria [8,9], resulting in increased cellular junctional permeability [11]. In addition, IAV infection and/or the related proinflammatory cytokine induction results in upregulation of trypsin, which induces marked increase in $[Ca^{2+}]_i$ and loss of zonula occudens-1 in endothelial cells via the protease-activated receptor 2 signaling [7]. Since fatty acid oxidation is a major energy pathway for ATP generation in mitochondria of endothelial cells [40,41], cells with disordered

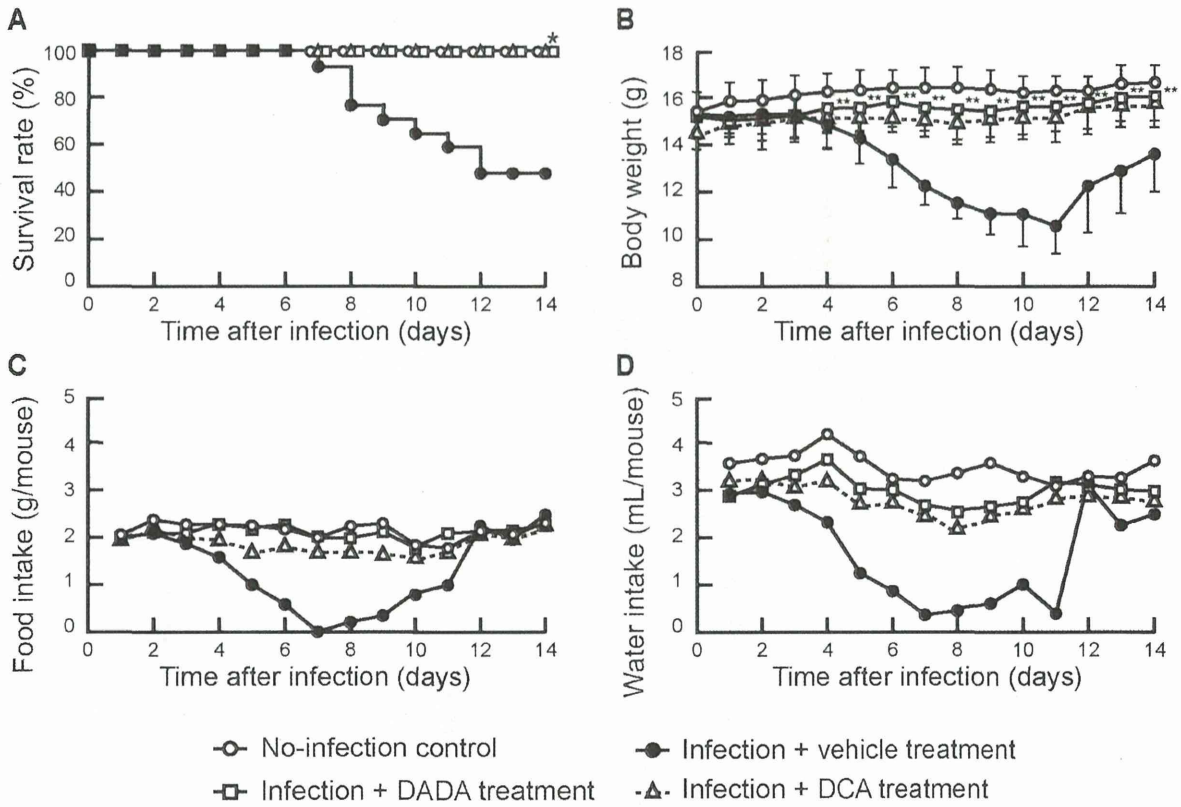


**Figure 8. Effects of DADA on survival rate, body weight, and food and water intake.** Mice infected with 60 pfu of IAV, representing the 50% lethal dose, were treated with oral DADA at 50 mg/kg, vehicle, or DCA administered peritoneally at 28 mg/kg at 12-h intervals for 14 days. The survival rate (A), body weight (B), food intake (C), and water intake (D) by infected mice were monitored. Differences in survival rate were analyzed by Kaplan-Meier and log-rank tests. Data are mean ± SD of 15 mice per group. *$P<0.05$, **$P<0.01$, vs. infected group treated with vehicle, by two-way ANOVA.
doi:10.1371/journal.pone.0098032.g008

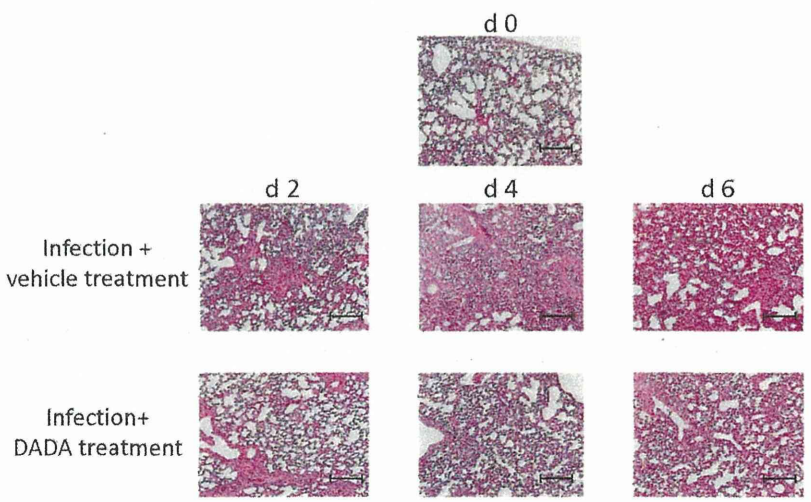


**Figure 9. Effects of DADA on pathological changes in the lungs.** Mice infected with 60 pfu of IAV were treated orally with DADA at 50 mg/kg or vehicle at 12-h intervals for 6 days. The lungs were isolated at days 0 (d0), 2 (d2), 4 (d4) or 6 (d6) post-infection, processed and stained with hematoxylin and eosin for histopathological evaluation. Each result is representative of 5 animals in each group. Bar, 300 μm.
doi:10.1371/journal.pone.0098032.g009

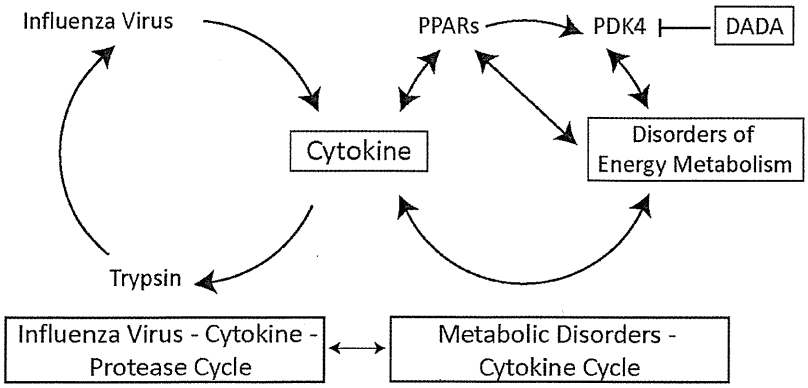


**Figure 10. Diagram illustrating the proposed pathogenic mechanism of MOF in severe influenza involving the host metabolic disorders–cytokine cycle linked to the influenza virus–cytokine–trypsin cycle.** PPARs, peroxisome proliferator-activated receptors; PDK4, pyruvate dehydrogenase kinase 4; DADA, diisopropylamine dichloroacetate.
doi:10.1371/journal.pone.0098032.g010

lipid metabolism suffer ATP depletion and dissociation of junctional complexes with increased permeability [42,43]. These results suggest that the lesser fuel utilization by the thermolabile compound variants of CPT II, a pivotal component of ATP generation through mitochondrial long-chain fatty acid oxidation, is an important etiological cause of acute brain edema and MOF during high fever in patients with influenza-associated encephalopathy [5,15,44].

As an extension to our previous studies, we added in the present study a new evidence for the marked up-regulation of PDK4 in IAV infection with suppression of PDH activity and ATP levels in the mitochondria, in addition to metabolic disorders and MOF in mice. It is well known that PDK4 is up-regulated by low food intake [18] and the pathological findings induced by IAV infection may be the complex outcome of viral proliferation, cytokine storm and PDK4 up-regulation associated with the lack of food intake after infection. The expression of PDK4 is transcriptionally regulated by PPARs (PPARα, PPARβ/δ, and PPARγ) in a tissue-specific manner [17,20,45,46]. Moseley and colleagues [33] reported that PPARγ and AMPK agonists provide protection in mice infected with highly pathogenic and pandemic strains of IAV. In the skeletal muscles and liver, the major resting energy expenditure organs in mammals [47], treatment with PPARγ and AMPK agonists reduces PDK4 expression in these organs, which increases glucose utilization and decreases the expression of genes involved in fatty acids transport and oxidation [45,48,49], although PPARγ agonists result in opposite increase in PDK4 expression in white adipose tissue [20]. These results support our finding that PDK4 inhibition by DADA and DCA significantly improved the survival of mice infected with severe IAV (Figure 8). Based on our new findings, together with the growing evidence of interrelation between cytokines and metabolic disorders [30–32], interrelation between cytokines and PPARs [33,46,50], and interrelation between PPARs and metabolic disorders through PDK4 [50–52], we propose a new concept of host cellular mechanism for MOF in severe influenza (Figure 10). This concept involves the metabolic disorders–cytokine cycle, which is interconnected with metabolite-mediated signaling pathways and transcription factors, such as PPARs, and PDK4, and in turn is closely linked to the influenza virus–cytokine–trypsin cycle for viral proliferation through cytokines. Coupling of these two cycles can explain the actions of DADA, through PDK4 inhibition, on normalization of glucose and lipid metabolism and ATP levels in the mitochondria, as well as suppression of cytokine production and viral replication in the lungs and trypsin up-regulation in various organs of mice infected with severe IAV (Figures 3–7), with resultant improvement in the survival rate (Figure 8).

Recent studies have demonstrated the involvement of mitochondria in a broad range of innate immune pathways, apart from the control of apoptosis, during infection [53]. Signaling molecules of antiviral immunity, such as mitochondrial antiviral signaling protein, IFN-β promoter stimulator 1, caspase-recruitment domain adaptor inducing IFN-β, and virus-induced signaling adaptor, are present on mitochondrial membranes and their activities are regulated by membrane potential ($\Delta\Psi_m$), ATP level and reactive oxygen species in the mitochondria [54]. Although the interaction between PDK4 and these signaling molecules on the membranes of mitochondria has not been elucidated so far, restoration of suppressed mitochondrial ATP levels and $\Delta\Psi_m$ in severe IAV infection by PDK4 inhibitors may augment mitochondria-derived antiviral immunity, resulting in suppression of IAV replication (Figure 6).

DADA-induced PDK4 inhibition produced marked suppression of IFN-α induction, but it caused only mild and insignificant inhibition of IFN-β (Figure 5). How can one explain these effects even though both cytokines are produced by the same type of cells and induced markedly and equally by IAV infection? While we cannot provide a solid explanation for this finding, the difference in DADA suppressive capacity on IFN-α and IFN-β may be due to the indirect inhibitory effects of DADA on cytokine production (see Figure 10). Further studies are required to determine the precise mechanisms of action of DADA on cytokine suppression.

Only the brain, among all the organs investigated in the present study, showed very mild or no pathological changes in PDH, PDK4 and ATP, except trypsin, in severe IAV infection. This sparing effect is probably related to the protective role of the blood-brain barrier against the transport of pathogenic molecules into the brain. However, trypsin in the brain is distributed mainly in cerebrovascular endothelial cells and hippocampal neuronal cells [12,38], and it is up-regulated in vascular endothelial cells by proinflammatory cytokines in the blood [7]. These findings suggest that the high levels of proinflammatory cytokines in the blood after IAV infection induce trypsin in cerebrovascular endothelial cells and DADA may suppress trypsin levels in the brain through down-regulation of cytokines. On the other hand, IAV infection and DADA treatment had no significant effects on trypsin expression

in the liver (Figure 7). The findings may be related to the high expression of anti-trypsin in the liver [55] and its effect of trypsin inhibition on the influenza virus–cytokine–trypsin cycle.

Among the known synthetic inhibitors of PDK, the pyruvate analog DCA is the most common classic inhibitor of PDK isoforms, including PDK4 [29,56]. DCA is known to have beneficial effects in inborn errors of mitochondrial metabolism, diabetes, lactic acidosis, myocardial ischemia and metabolism of cancer cells to increase mitochondrial-dependent apoptosis [29,57–59]. However, DCA also has symptomatic adverse reaction of peripheral neuropathy [23,60,61]. In the present study, DADA, a new PDK4 inhibitor, inhibited PDK4 and PDK2 with potency similar to DCA (Table 3). DADA was originally obtained from apricot nuclei and called pangamic acid or "vitamin B15" [21] and has been used as a safety treatment option for hepatic injury and nonalcoholic fatty liver diseases [62] without symptomatic peripheral neuropathy or other adverse effects. The present study suggests that DADA is an alternative and safe PDK4 inhibitor, potentially suitable for treatment of MOF in severe IAV infection.

## Acknowledgments

We thank Dr. M. Horiuchi for the kind supply of antibodies against PDK4.

## Author Contributions

Conceived and designed the experiments: HK MH. Performed the experiments: KY ILI JC YY. Analyzed the data: KY ILI JC YY. Contributed reagents/materials/analysis tools: HK KY ILI. Wrote the paper: KY HK.

## References


1. Lipatov MS, Govorkova EA, Webby RJ, Ozaki H, Peiris M, et al. (2004) Influenza: emergence and control. J Virol 78: 8951–8959.
2. Kim HW, Brandt CD, Arrobio JO, Murphy B, Chanock RM, et al. (1979) Influenza A and B virus infection in infants and young children during the years 1957–1976. Am J Epidemiol 109: 464–479.
3. Chowell G, Echevarria-Zuno S, Viboud C, Simonsen L, Miller MA, et al. (2012) Epidemiological Characteristics and Underlying Risk Factors for Mortality during the Autumn 2009 Pandemic Wave in Mexico. PLoS One 7: e41069. Available: http://www.plosone.org/article/info%3Adoi%2F10.1371%2Fjournal.pone.0041069.
4. Delorme L, Middleton PL (1979) Influenza A virus associated with acute encephalopathy. Am J Dis Child 133: 822–824.
5. Yao D, Mizuguchi H, Yamaguchi M, Yamada H, Chida J, et al. (2008) Thermal instability of compound variants of carnitine palmitoyltransferase II and impaired mitochondrial fuel utilization in influenza-associated encephalopathy. Hum Mutat 29: 718–727.
6. Perkins LE, Swayne DE (2001) Pathobiology of A/chicken/Hong Kong/220/97 (H5N1) avian influenza virus in seven gallinaceous species. Vet Pathol 38: 149–164.
7. Wang S, Le TQ, Kurihara N, Chida J, Cisse Y, et al. (2010) Influenza virus-cytokine-protease cycle in the pathogenesis of vascular hyperpermeability in severe influenza. J Infect Dis 202: 991–1001.
8. Spraque AH, Khalil RA (2009) Inflammatory cytokines in vascular dysfunction and vascular disease. Biochem Pharmacol 78: 539–552.
9. Mariappan N, Elks CM, Fink B, Francis J (2009) TNF-induced mitochondrial damage: a link between mitochondrial complex I activity and left ventricular dysfunction. Free Radic Biol Med 46: 462–470.
10. Mizuguchi M, Yamanouchi H, Ichiyama T, Shiomi M (2007) Acute encephalopathy associated with influenza and other viral infections. Acta Neurol Scand Suppl 186: 45–56.
11. Denker BM, Nigam SK (1998) Molecular structure and assembly of the tight junction. Am J Physiol 274: F1–F9.
12. Kido H, Okumura Y, Takahashi E, Pan HY, Wang S, et al. (2012) Role of host cellular proteases in the pathogenesis of influenza and influenza-induced multiple organ failure. Biochim Biophys Acta 1824: 186–194.
13. Pan HY, Yamada H, Chida J, Wang S, Yano M, et al. (2011) Up-regulation of ectopic trypsins in the myocardium by influenza A virus infection triggers acute myocarditis. Cardiovasc Res 58: 19–28.
14. Pan HY, Yano M, Kido H (2011) Effects of inhibitors of Toll-like receptors, protease-activated receptor-2 signalings and trypsin on influenza A virus replication and upregulation of cellular factors in cardiomyocytes. J Med Invest 58: 19–28.
15. Chen Y, Mizuguchi H, Yao D, Ide M, Kuroda Y, et al. (2005) Thermolabile phenotype of carnitine palmitoyltransferase II variations as a predisposing factor for influenza-associated encephalopathy. FEBS Lett 579: 2040–2044.
16. Yao D, Yao M, Yamaguchi M, Chida J, Kido H (2011) Characterization of compound missense mutation and deletion of carnitine palmitoyltransferase II in a patient with adenovirus-associated encephalopathy. J Med Invest 58: 210–218.
17. Sugden MC, Holness MJ (2003) Recent advances in mechanisms regulating glucose oxidation at the level of the pyruvate dehydrogenase complex by PDKs. Am J Physiol Endocrinol Metab 284: E855–E862.
18. Harris RA, Bowker-Kinley MM, Huang B, Wu P (2002) Regulation of the activity of the pyruvate dehydrogenase complex. Adv Enzyme Regul 42: 249–259.
19. Bowker-Kinley MM, Davis WI, Wu P, Harris RA, Popov KM (1998) Evidence for existence of tissue-specific regulation of the mammalian pyruvate dehydrogenase complex. Biochem J 329: 191–196.
20. Jeong JY, Jeoung NH, Park KG, Lee IK (2012) Transcriptional regulation of pyruvate dehydrogenase kinase. Diabetes Metab J 36: 328–335.
21. Herbert V (1979) Pangamic acid ("vitamin B15"). Am J Clin Nutr 32: 1534–1540.
22. Naito E, Kuroda Y, Toshima K, Takeda E, Saijo T, et al. (1989) Effect of sodium dichloroacetate on human pyruvate metabolism. Brain Dev 11: 195–197.
23. Stacpoole PW, Kerr DS, Barnes C, Bunch ST, Carney PR, et al. (2006) Controlled clinical trial of dichloroacetate for treatment of congenital lactic acidosis in children. Pediatrics 117: 1519–1531.
24. Chida J, Yamane K, Takei T, Kido H (2012) An efficient extraction method for quantitation of adenosine triphosphate in mammalian tissues and cells. Anal Chim Acta 727: 8–12.
25. Chida J, Ono R, Yamane K, Hiyoshi M, Nishimura M, et al. (2013) Blood lactate/ATP ratio, as an alarm index and real-time biomarker in critical illness. PLoS One 8: e60561.
26. Kitagawa D, Yokota K, Gouda M, Narumi Y, Ohmoto H, et al. (2013) Activity-based kinase profiling of approved tyrosine kinase inhibitors. Genes Cells 18: 110–122.
27. Ushikai M, Horiuchi M, Kobayashi K, Matuda S, Inui A, et al. (2011) Induction of PDK4 in the heart muscle of JVS mice, an animal model of systemic carnitine deficiency, does not appear to reduce glucose utilization by the heart. Mol Genet Metab 102: 349–355.
28. Kato M, Li J, Chuang JL, Chuang DT (2007) Distinct structural mechanisms for inhibition of pyruvate dehydrogenase kinase isoforms by AZD7545, dichloroacetate, and radicicol. Structure 15: 992–1004.
29. Bersin RM, Stacpoole PW (1997) Dichloroacetate as metabolic therapy for myocardial ischemia and failure. Am Heart J 134: 841–855.
30. Hardaway AL, Podgorski I (2013) IL-1β, RAGE and FABP4: targeting the dynamic trio in metabolic inflammation and related pathologies. Future Med Chem 5: 1089–1108.
31. Lee H, Lee IS, Choue R (2013) Obesity, inflammation and diet. Pediatr Gastroenterol Hepatol Nutr 16: 143–152.
32. Close TE, Cepinskas G, Omatsu T, Rose KL, Summers K, et al. (2013) Diabetic ketoacidosis elicits systemic inflammation associated with cerebrovascular endothelial cell dysfunction. Microcirculation 20: 534–543.
33. Moseley CE, Webster RG, Aldridge JR (2010) Peroxisome proliferator-activated receptor and AMP-activated protein kinase agonists protect against lethal influenza virus challenge in mice. Influenza Other Respi Viruses 4: 307–311.
34. Fedson DS (2009) Confronting the next influenza pandemic with anti-inflammatory and immunomodulatory agents: why they are needed and how they might work. Influenza Other Respi Viruses 3: 129–142.
35. Yang B, Yao D, Ohuchi M, Ide M, Yano M, et al. (2002) Ambroxol suppresses influenza-virus proliferation in the mouse airway by increasing antiviral factor levels. Eur Respir J 19: 952–958.
36. Yamada H, Le QT, Kousaka A, Higashi Y, Tsukane M, et al. (2006) Sendai virus infection up-regulates trypsin I and matrix metalloproteinase-9, triggering viral multiplication and matrix degradation in rat lungs and lung L2 cells. Arch Virol 151: 2529–2537.
37. Towatari T, Ide M, Ohba K, Chiba Y, Murakami M, et al. (2002) Identification of ectopic anionic trypsin I in rat lungs potentiating pneumotropic virus infectivity and increased enzyme level after virus infection. Eur J Biochem 269: 2613–2621.
38. Le TQ, Kawachi M, Yamada H, Shiota M, Okumura Y, et al. (2006) Identification of trypsin I as a candidate for influenza A virus and Sendai virus envelope glycoprotein processing protease in rat brain. Biol Chem 387: 467–475.
39. Basler CF (2007) Influenza viruses: basic biology and potential drug targets. Infect Disord Drug Targets 7: 282–293.
40. Dagher Z, Ruderman N, Tornheim K, Ido Y (2001) Acute regulation of fatty acid oxidation and amp-activated protein kinase in human umbilical vein endothelial cells. Circ Res 88: 1276–1282.
41. Oldendorf WH, Cornford ME, Brown WJ (1977) The large apparent work capability of the blood-brain barrier: a study of the mitochondrial content of

capillary endothelial cells in brain and other tissues of the rat. Ann Neurol 1: 409–417.
42. Plateel M, Dehouck MP, Torpier G, Cecchelli R, Teissier E (1995) Hypoxia increases the susceptibility to oxidant stress and the permeability of the blood-brain barrier endothelial cell monolayer. J Neurochem 65: 2138–2145.
43. Witt KA, Mark KS, Hom S, Davis TP (2003) Effects of hypoxia-reoxygenation on rat blood-brain barrier permeability and tight junctional protein expression. Am J Physiol Heart Circ Physiol 285: H2820–H2831.
44. Yao M, Yao D, Yamaguchi M, Chida J, Yao D, et al. (2011) Bezafibrate upregulates carnitine palmitoyltransferase II expression and promotes mitochondrial energy crisis dissipation in fibroblasts of patients with influenza-associated encephalopathy. Mol Genet Metab 104: 265–272.
45. Way JM, Harrington WW, Brown KK, Gottschalk WK, Sundseth SS, et al. (2001) Comprehensive messenger ribonucleic acid profiling reveals that peroxisome proliferator-activated receptor gamma activation has coordinate effects on gene expression in multiple insulin-sensitive tissues. Endocrinology 142: 1269–1277.
46. Gallagher D, Belmonte D, Deurenberg P, Wang Z, Krasnow N, et al. (1998) Organ-tissue mass measurement allows modeling of REE and metabolically active tissue mass. Am J Physiol 275: E249–E258.
47. Kim YD, Kim YH, Tadi S, Yu JH, Jeoung NH, et al. (2012) Metformin inhibits growth hormone-mediated hepatic PDK4 gene expression through induction of orphan nuclear receptor small heterodimer partner. Diabetes 61: 2484–2494.
48. McAinch AJ, Cameron-Smith D (2009) Adiponectin decreases pyruvate dehydrogenase kinase 4 gene expression in obese- and diabetic-derived myotubes. Diabetes Obes Metab 11: 721–728.
49. da Rocha Junior LF, Dantas AT, Duarte AL, de Melo Rego MJ, Pitta Ida R, et al. (2013) PPARγ agonists in adaptive immunity: what do immune disorders and their models have to tell us? PPAR Res 2013:519724.
50. Nakamura MT, Yudell BE, Loor JJ (2014) Regulation of energy metabolism by long-chain fatty acids. Prog Lipid Res 53: 124–144.
51. Kelly DP (2003) PPARs of the heart: three is a crowd. Circ Res 92: 482–484.
52. Planavila A, Sánchez RM, Merlos M, Laguna JC, Vázquez-Carrera M (2005) Atorvastatin prevents peroxisome proliferator-activated receptor γ coactivator-1 (PGC-1) downregulation in lipopolysaccharide-stimulated H9c2 cells. Biochim Biophys Acta 1736: 120–127.
53. West AP, Shadel GS, Ghosh S (2011) Mitochondria in innate immune responses. Nat Rev Immunol 11: 389–402.
54. Koshiba T (2013) Mitochondrial-mediated antiviral immunity. Biochim Biophys Acta 1833: 225–232.
55. Hunt JM, Tuder R (2012) Alpha 1 anti-trypsin: one protein, many functions. Curr Mol Med 12: 827–835.
56. Whitehouse S, Cooper RH, Randle PJ (1974) Mechanism of activation of pyruvate dehydrogenase by dichloroacetate and other halogenated carboxylic acids. Biochem J 141: 761–774.
57. Henderson GN, Yan Z, James MO, Davydova N, Stacpooles PW (1997) Kinetics and metabolism of chloral hydrate in children: identification of dichloroacetate as a metabolite. Biochem Biophys Res Commun 235: 695–698.
58. Stacpoole PW (1989) The pharmacology of dichloroacetate. Metabolism 38: 1124–1144.
59. Sutendra G, Michelakis ED (2013) Pyruvate dehydrogenase kinase as a novel therapeutic target in oncology. Front Oncol 3: 38.
60. Kaufmann P, Engelstad K, Wei Y, Jhung S, Sano MC, et al. (2006) Dichloroacetate causes toxic neuropathy in MELAS: a randomized, controlled clinical trial. Neurology 66: 324–330.
61. Stacpoole PW, Nagaraja NV, Hutson AD (2003) Efficacy of dichloroacetate as a lactate-lowering drug. J Clin Pharmacol 43: 683–691.
62. Lu LG, Zeng MD, Mao YM, Chen CW, Fu QC, et al. (2005) Diisopropylamine dichloroacetate in the treatment of nonalcoholic fatty liver disease: a multicenter random double-blind controlled trial. Zhonghua Gan Zang Bing Za Zhi 13: 92–95.

Arch Virol (2015) 160:225–234
DOI 10.1007/s00705-014-2270-5

ORIGINAL ARTICLE

# Influenza A virus infection of vascular endothelial cells induces GSK-3β-mediated β-catenin degradation in adherens junctions, with a resultant increase in membrane permeability

**M. Hiyoshi · I. L. Indalao · M. Yano · K. Yamane · E. Takahashi · H. Kido**

Received: 25 June 2014 / Accepted: 25 October 2014 / Published online: 12 November 2014


**Abstract** Multiorgan failure with vascular hyperpermeability is the final outcome in the progression of seasonal influenza virus pneumonia and influenza-associated encephalopathy, and it is also common in infection with highly pathogenic avian influenza virus. However, the precise molecular mechanism by which influenza virus infection causes vascular endothelial cell hyperpermeability remains poorly defined. We investigated the mechanisms of hyperpermeability of human umbilical vein endothelial cells infected with influenza A virus (IAV)/Puerto Rico/8/34 (PR8) (H1N1). The levels of β-catenin, a key regulatory component of the vascular endothelial-cadherin cell adhesion complex, were markedly decreased during infection for 28 h, with increments of vascular hyperpermeability measured by transendothelial electrical resistance. Lactacystin (at 2 μM), a proteasome inhibitor, inhibited the decrease in β-catenin levels. Since the N-terminal phosphorylation of β-catenin by glycogen synthase kinase (GSK)-3β is the initiation step of proteasome-dependent degradation, we examined the effects of GSK-3β suppression by RNA interference in endothelial cells. IAV-infection-induced β-catenin degradation was significantly inhibited in GSK-3β-knockdown cells, and transfection of cells with recombinant β-catenin significantly suppressed IAV-induced hyperpermeability. These findings suggest that IAV infection induces GSK-3β-mediated β-catenin degradation in the adherens junctional complexes and induces vascular hyperpermeability. The *in vitro* findings of β-catenin degradation and activation of GSK-3β after IAV infection were confirmed in lungs of mice infected with IAV PR8 during the course of infection from day 0 to day 6. These results suggest that GSK-3β-mediated β-catenin degradation in adherens junctions is one of the key mechanisms of vascular hyperpermeability in severe influenza.

## Introduction

Influenza A virus (IAV) is the most common infectious pathogen in humans and causes significant morbidity and mortality, particularly in infants and the elderly population [1, 2]. Multiorgan failure (MOF) with vascular hyperpermeability is reported in the progressive stage of seasonal influenza virus pneumonia, particularly in patients with underlying risk factors [3], and is also common in infections caused by highly pathogenic avian influenza virus [4]. Vascular hyperpermeability caused by destruction of a tight junction constituent, zonula occludens-1 (ZO)-1, of the blood-brain-barrier (BBB) in brain endothelial cells is also reported in influenza-associated encephalopathy in infancy and early childhood in East Asians [5–8]. We reported previously that the "influenza–cytokine–trypsin and matrix metalloprotease-9" cycle is a key pathogenic

M. Hiyoshi, I. L. Indalao and M. Yano contributed equally to this work.

M. Hiyoshi · I. L. Indalao · M. Yano · K. Yamane · E. Takahashi · H. Kido (✉)
Division of Enzyme Chemistry, Institute for Enzyme Research, The University of Tokushima, Kuramoto-cho 3-18-15, Tokushima 770-8503, Japan
e-mail: kido@tokushima-u.ac.jp

*Present Address:*
M. Hiyoshi
Department of Biochemistry, Shimane University Faculty of Medicine, Izumo, Shimane 693-8501, Japan

*Present Address:*
M. Yano
Department of Nutrition, School of Human Cultures, The University of Shiga Prefecture, Hikone, Shiga 522-8533, Japan

mechanism in the interaction between IAV infection and vascular endothelial cells and their hyperpermeability in severe influenza [8, 9].

The state of hypercytokinemia in IAV infection (e.g., high levels of tumor necrosis factor, interleukin 6, and interleukin-1β), called a "cytokine storm", affects cell adhesion, permeability, apoptosis, and mitochondrial energy metabolism and reactive oxygen species, potentially resulting in vascular dysfunction, hyperpermeability and MOF [10, 11], although their precise mechanisms have not been elucidated so far. Furthermore, IAV infection induces upregulation of trypsin and matrix metalloprotease-9 through an "influenza–cytokine–protease" cycle in various organs and vascular endothelial cells [8, 9, 11, 12], and an increase in the levels of these proteases in the extracellular space caused by this cycle results in the degradation of vascular basement membranes and the extracellular matrix, resulting in vascular hyperpermeability and inflammatory cell migration. Trypsin promotes viral entry and replication because IAV does not encode a viral hemagglutinin processing protease in its own genes, and post-transcriptional hemagglutinin cleavage by cellular trypsin-type proteases is needed for membrane fusion activity, virus entry into cells, and multiple cycles of viral replication [13–15]. In addition, trypsin evokes cytokine release via the proteinase-activated receptor (PAR)-2 [16] and also plays a role in BBB destruction by increasing intracellular calcium concentrations ($[Ca^{2+}]_i$) and loss of tight-junction protein ZO-1 via PAR-2 in the BBB [8, 17].

For the control of vascular permeability, there is another major type of cell-to-cell junction, the adherens junction, which is ubiquitously distributed along the vascular tree and is expressed in both blood and lymphatic vessels [18]. The adherens junction is formed by the transmembrane adhesion molecule vascular endothelial (VE)-cadherin and its cytoplasmic tail binding molecules, β-catenin and plakoglobin, which anchor to actin via α-catenin and stabilize the junction [19].

In this study, we investigated the mechanisms of IAV-induced disruption of adherens junctions and vascular hyperpermeability in human endothelial cells *in vitro* and confirmed these findings *in vivo*. We found that GSK-3β-mediated β-catenin degradation in the VE-cadherin complex in the adherens junction of human endothelial cells was associated with increased hyperpermeability after IAV infection.

## Materials and methods

### Cell culture

Normal human umbilical vein endothelial cells (HUVECs) (Kurabo Industries, Osaka, Japan) on type-I-collagen-coated dishes (10 cm diameter) were grown in HuMedia-EG2 culture medium using the protocol supplied by the manufacturer. The cells were cultured in a humidified atmosphere of 5 % $CO_2$–95 % air gas mixture at 37 °C.

### Influenza A virus infection

IAV/PR/8/34 (H1N1) was provided by the Research Foundation for Microbial Diseases of Osaka University (Kagawa, Japan). Before infection of HUVEC with IAV PR8, the culture medium was replaced with serum-free HuMedia-EB2 infection medium containing 0.1 % bovine serum albumin (BSA). The cells were infected with IAV PR8 at a multiplicity of infection (MOI) of 1. After incubation for 1 h, the infection medium was replaced with a culture medium containing various reagents, and the cells were incubated for another 28 h.

For animal experiments, specified-pathogen-free 4-week-old weanling C57BL/6CrSlc female mice were obtained from Japan SLC and maintained in a 12-h light/dark cycle in a temperature-controlled room with free access to food and water. All animals were treated according to the Guide for the Care and Use of Laboratory Animals (NIH Publication No. 85-23, 1996), and the study was approved by the Animal Care Committee of the University of Tokushima. Under ketamine and xylazine anesthesia, 100 plaque-forming units of IAV PR8 in 20 μL of saline or saline alone as an uninfected control was instilled intranasally in mice. Body weight and survival were monitored daily, and the animals were assessed visually for signs of clinical disease including inactivity, ruffled fur, labored respiration and huddling behavior. Mice that lost ≥30 % of their original body weight and/or displayed evidence of pneumonia were sacrificed by overdose of intraperitoneal ketamine and xylazine. These experiments were conducted under animal BSL2 conditions.

### Western immunoblotting

HUVECs after various treatments were lysed in radioimmunoprecipitation assay (RIPA) buffer (50 mM Tris-HCl, pH 8.0, 150 mM NaCl, 10 % glycerol, 1 % NP 40, 0.5 % deoxycholate, 0.4 mM EDTA, and 0.5 mM sodium orthovanadate) for 30 min at 4 °C. Mouse lungs isolated during the course of IAV infection (from day 0 to day 6) were homogenized with five volumes of RIPA buffer. Cell lysate and lung homogenate were centrifugation at 10,000×*g* for 30 min. The prepared cell lysates (20 μg protein/lane) and lung extracts (20 μg protein/lane) were separated by sodium dodecyl sulfate polyacrylamide gel electrophoresis (SDS-PAGE) using 10-to-20 % gradient gel and transferred onto an Immobilon-P membrane (Millipore, Bedford, MA). After blocking with 5 % non-fat milk in 20 mM

Tris-HCl, pH 7.5, 150 mM NaCl and 0.05 % Tween 20, the membranes were incubated with optimal primary antibodies for 2 h. The primary antibodies included anti-β-catenin, anti-VE-cadherin, anti-β-actin and anti-glycogen synthase kinase (GSK)-3β (all from Santa Cruz Biotechnology, Santa Cruz, CA), anti-phospho-GSK-3β (Ser9) (Cell Signaling Technology, Beverly, MA) and anti-IAV (Takara). Thereafter, peroxidase-conjugated anti-mouse (Invitrogen, Carlsbad, CA), -rabbit (Sigma, St. Louis, MO) or -goat (Sigma) IgG antibodies were incubated for 30 min, followed by enhanced chemiluminescence reagents (GE Healthcare Biosciences, Uppsala, Sweden) for 1 min.

### Reverse transcription polymerase chain reaction (RT-PCR)

Total RNA was extracted from HUVECs using an RNeasy Mini Kit (QIAGEN, Hilden, Germany). RT-PCR was carried out using a One-Step RT-PCR Kit (QIAGEN) according to the instructions provided by the manufacturer. To amplify the PCR product of β-catenin, the following primer pair was used (forward primer, 5′-TTTGGCTGAA CCATCACAGA-3′; and reverse primer, 5′-TGTTGAG CAAGGCAACCATT-3′). The products were examined by agarose gel electrophoresis after 25 cycles.

### Relative quantitation analysis

Protein or mRNA bands detected on X-ray films or pictures were calculated by densitometric analysis using Just TLC (Sweday, Lund, Sweden). The relative levels of the immunoblot or RT-PCR bands were expressed as mean values ±SD.

### RNA interference

The sequence of the sense strand used to generate specific siRNA was obtained as follows: GSK-3β, NCBI Reference Sequence: NG_012922.1, 5′-AAATCTCTTGTCCTGCA ATAC-3′. A small interfering RNA (siRNA) was synthesized using a Silencer siRNA Construction Kit (Ambion, Austin, TX) according to the instructions supplied by the manufacturer. HUVECs were transfected with the siRNA at 10 nM, using Oligofectamine Transfection Reagent (Invitrogen) and grown for 72 h to allow sufficient decrease in the expression of this molecule.

### Assessment of hyperpermeability by trans-endothelial electrical resistance (TEER) and transfection with recombinant β-catenin

HUVEC were plated in the upper chamber of type I collagen-coated cell culture inserts with a membrane of 3.0 μm pore size. After infection of the cells with IAV PR8 at a MOI of 1 for 24 h, some of the cells on the plates were transfected with recombinant β-catenin (1.2 μg/mL) (Millipore). Recombinant β-catenin was exposed to the transfection reagent TransIT-LT1 polyamine (Mirus, Madison, WI) for 15 min before transfection. After transfection for 4 h, the TEER across monolayers of endothelial cells was measured using Millicell-ERS (Millipore) using the method described previously [20, 21]. The electrical resistance of blank inserts containing the medium only was subtracted from the TEER measurements made from inserts containing confluent endothelial cell monolayers.

### Statistical analysis

The mean values ±SD of individual groups were calculated, and the differences between groups were analyzed using the unpaired *t*-test or multiple comparisons (Bonferroni or Dunnett tests) after one-way analysis of variance (ANOVA). All statistical analyses were performed using Microsoft Excel (Microsoft, Redmond, WA) add-in Ekuseru-Toukei 2010 version 1.10 (Social Survey Research Information Co.). All values are two-tailed and those less than 0.05 were considered statistically significant.

## Results

### IAV infection downregulates β-catenin significantly, but not VE-cadherin, in adherens junctional proteins in HUVECs

Figures 1A and B show the results of immunoblotting analyses of β-catenin and VE-cadherin, the major adherens junctional proteins, in HUVECs infected with IAV PR8 at an MOI of 1 for 28 h or in uninfected cells. Infection significantly suppressed the expression of β-catenin to 24 % of the no-infection control ($P < 0.0001$). The expression of the transmembrane adhesive component VE-cadherin also tended to decrease, though not significantly, after infection ($P = 0.2472$). Quantitative RT-PCR analysis showed a slight, but significant, decrease in the β-catenin mRNA level to 84 % of the no-infection control ($P = 0.0188$) in infected HUVECs (Fig. 1C and D). The discrepancy between the suppression levels of β-catenin protein and those of β-catenin mRNA after IAV infection indicates that the marked suppression of the β-catenin protein level was probably due to enhanced β-catenin protein degradation.

### Lactacystin inhibits IAV-induced β-catenin degradation

To verify the above-stated findings, HUVECs were treated with 2 μM lactacystin (Sigma), a proteasome inhibitor

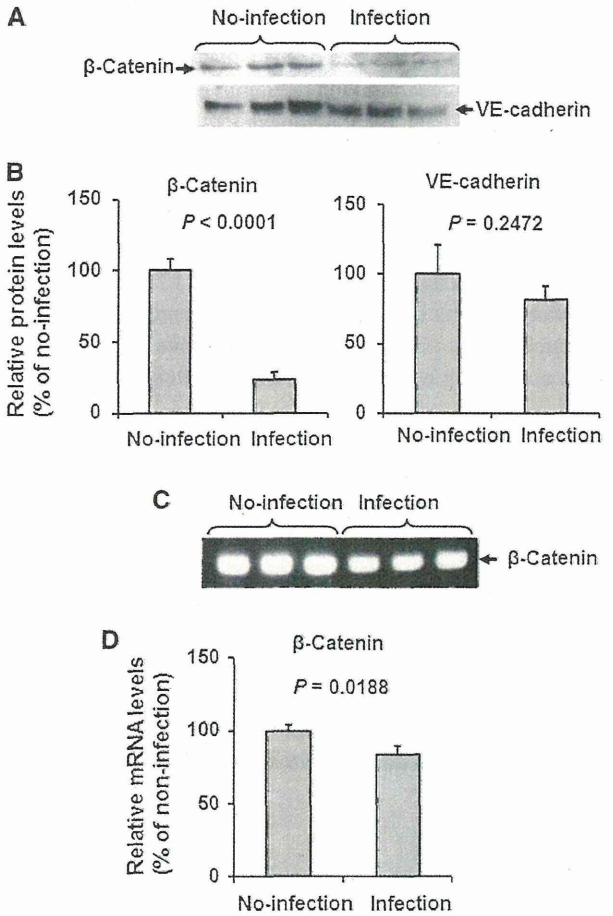


**Fig. 1** Infection with IAV reduces the expression of β-catenin in adherens junctional proteins in HUVECs. **A.** Representative immunoblot (from three separate experiments) of β-catenin and VE-cadherin in cell lysates (20 μg protein/lane) of HUVECs after infection for 28 h with or without IAV PR8. As a control, saline was used as no-infection agent. **B.** Relative levels of β-catenin and VE-cadherin in the blot in panel A (n = 3), determined as described in Materials and methods. Statistical analysis was performed using the unpaired *t*-test. **C.** Representative RT-PCR data of β-catenin in control (uninfected) and IAV-infected HUVECs at 28 h post-transfection. D: Relative levels of β-catenin in the RT-PCR experiment shown in panel C (n = 3). Statistical analyses were conducted using the unpaired *t*-test

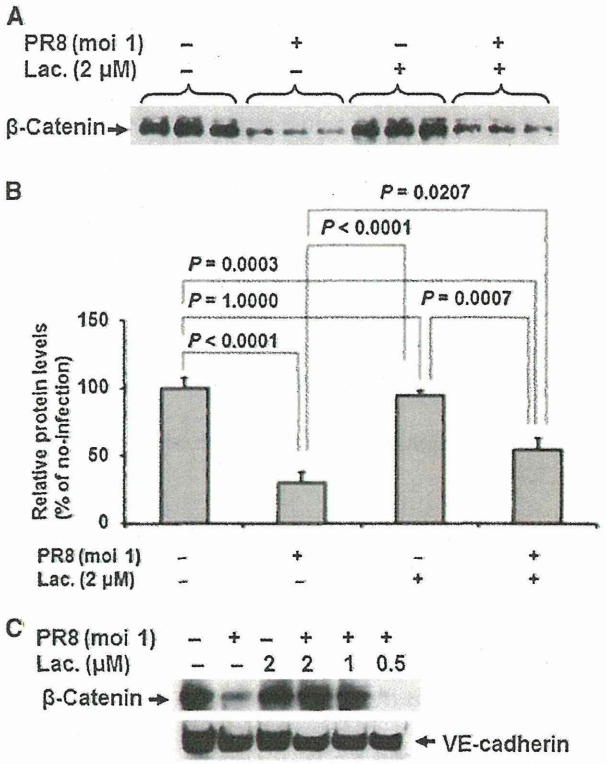


**Fig. 2** Lactacystin inhibits IAV-induced β-catenin suppression. **A.** Representative immunoblot (from three separate experiments) of β-catenin in cell lysates (20 μg protein/lane) of control (uninfected) or IAV-infected HUVECs treated with or without lactacystin for 28 h. **B.** Relative level of β-catenin in the blot in panel A (n = 3). Multiple comparisons tests (Bonferroni test after one-way analysis of variance (ANOVA) were used for statistical analysis. **C.** Dose-response effect of lactacystin on β-catenin and VE-cadherin expression. HUVECs were treated with various concentrations of lactacystin (from 0 to 2 μM) at the time of infection and then incubated for 28 h. A representative immunoblot of β-catenin and VE-cadherin in cell lysates (20 μg protein/lane) with or without infection is shown

[22], at the time of PR8 infection and the cells were incubated for 28 h. Under no-infection conditions, lactacystin did not affect β-catenin protein levels in HUVEC ($P = 1.0000$) (Fig. 2A and B). In contrast, lactacystin significantly abrogated the suppression of the β-catenin protein level in IAV PR8-infected HUVECs ($P = 0.0207$), and the levels were 1.8-fold higher than those in infected cells that were not treated with lactacystin. The inhibitory effect of lactacystin was dose-dependent, and lactacystin at 0.5 μM was not enough to restore the β-catenin levels (Fig. 2C). Expression of VE-cadherin was not affected by treatment with various doses of lactacystin. These results confirmed that the downregulation of the β-catenin protein level in IAV PR8-infected HUVECs is the result of enhanced proteasomal degradation.

## IAV PR8 infection activates GSK-3β in HUVECs

β-Catenin, which is phosphorylated by GSK-3β at residues 37 and 33, is recognized by the β-TrCP E3-ligase complex, ubiquitylated, and rapidly degraded by the 26S proteasome [23, 24]. To elucidate the mechanism(s) of enhanced β-catenin degradation in HUVEC by IAV infection, the expression level of the active form of dephosphorylated GSK-3β (Ser9) was analyzed by western immunoblotting using specific antibodies against GSK-3β and phospho-GSK-3β (Ser9) to detect the inactive form of phosphorylated GSK-3β (Fig. 3A and B). The total amount of GSK-3β in IAV PR8-infected cells was only

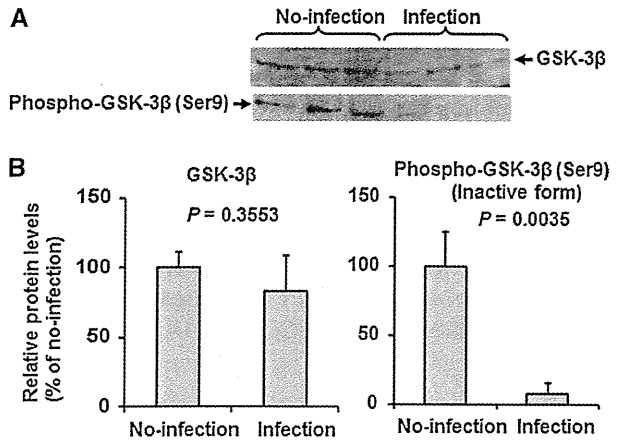


**Fig. 3** IAV infection induces suppression of phosphorylated GSK-3β in HUVECs. **A.** Representative immunoblots (from three separate experiments) of total GSK-3β and phosphor-GSK-3β (Ser9) in cell lysates (20 μg protein/lane) of control (uninfected) or IAV-infected HUVECs. **B.** Relative levels of total GSK-3β and phosphor-GSK-3β (Ser9) in the blot in panel A (n = 3). Data are mean ± SD. Statistical analyses were conducted using the unpaired *t*-test

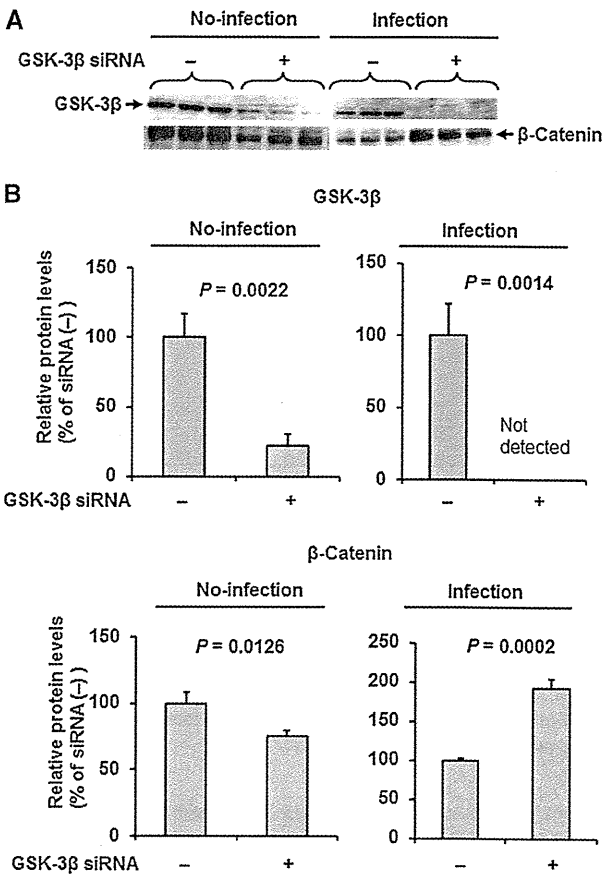


**Fig. 4** GSK-3β knockdown protects against IAV-induced suppression of β-catenin. **A.** Representative immunoblots (from three separate experiments) of GSK-3β and β-catenin in cell lysates (20 μg protein/lane) of HUVECs pre-treated with or without GSK-3β knockdown under control (no-infection) and IAV-infection conditions. **B.** Relative levels of GSK-3β and β-catenin in the bolt in panel A (n = 3). Differences between groups were analyzed using the unpaired *t*-test

slightly decreased to 83 % of the no-infection control cells, and the decrease was not significant ($P = 0.3553$). In contrast, IAV infection markedly decreased the level of the phosphorylated-GSK-3β (Ser9) form to 8 % ($P = 0.0035$). These results indicate that IAV infection induces GSK-3β in HUVECs from the inactive phosphorylated-GSK-3β (Ser9) form to the active dephosphorylated-GSK-3β (Ser9) form.

## GSK-3β knockdown protects against IAV infection-induced suppression of β-catenin expression

Since degradation of β-catenin, a major component of the VE-cadherin complex, is initiated by the activation of GSK-3β, we next analyzed the effects of GSK-3β gene-silencing on the level of β-catenin in IAV-infected and uninfected HUVECs (Fig. 4A and B). HUVECs treated with or without GSK-3β knockdown were infected with IAV PR8 at a MOI of 1 and β-catenin levels in the cells were measured by western immunoblotting at 28 h post-infection. Under no-infection conditions, GSK-3β knockdown treatment resulted in suppression of GSK-3β expression in HUVEC to about 20 % of the level without treatment. Although GSK-3β expression was downregulated in HUVECs by IAV infection, the expression was further suppressed by GSK-3β gene silencing to an undetectable level. The β-catenin expression level in HUVECs treated with GSK-3β knockdown under no-infection conditions was 76 % of those without knockdown treatment ($P = 0.0126$). However, the β-catenin expression level in GSK-3β knockdown cells was 1.9-fold of that in HUVECs without treatment under infection conditions ($P = 0.0002$). These data suggest that the β-catenin level in the VE-cadherin complex is strictly regulated by GSK-3β in IAV-infected HUVECs.

## Transfection with β-catenin restores the IAV-infection-disrupted barrier function

The hyperpermeability of monolayers of HUVECs was measured by TEER. Infection of HUVECs with IAV PR8 at an MOI of 1 for 24 h resulted in a significant decrease in TEER ($P = 0.0367$), indicating cell hyperpermeability (Fig. 5). Transfection of the vehicle (TransIT-LT1 polyamine) tended to reduce TEER, albeit insignificantly ($P = 0.5409$). However, pretreatment of HUVECs by transfection with recombinant β-catenin for 4 h markedly increased TEER ($P = 0.0003$), and the monolayer

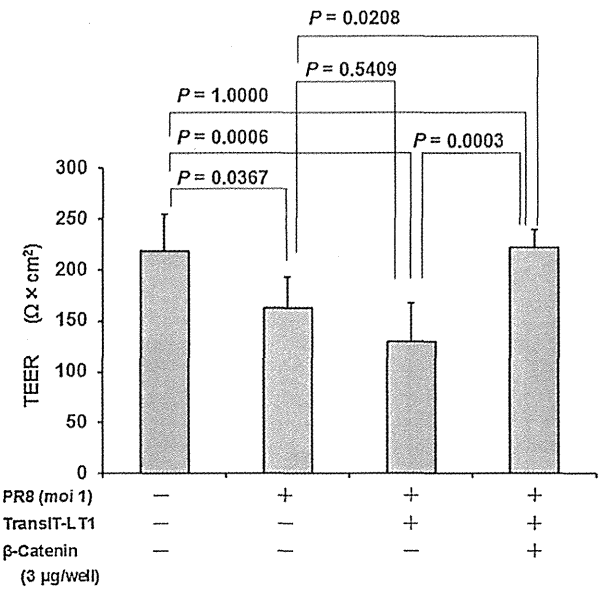


**Fig. 5** Transfection with recombinant β-catenin abrogates IAV infection-induced impairment of barrier function. TEER data across monolayers of control (uninfected) and IAV-infected HUVECs (n = 6), and with or without recombinant β-catenin transfection were analyzed using multiple comparison (Bonferroni test) after one-way analysis of variance (ANOVA)

permeability was almost completely restored to the levels recorded in uninfected and untransfected cells.

### Changes in expression levels of adherens junctional proteins and GSK-3β in lungs of mice infected with IAV PR8

The time courses of change in β-catenin, VE-cadherin, GSK-3β, phospho-GSK-3β (Ser 9) and viral nucleoprotein (NP) expression levels were analyzed in the lungs of mice infected intranasally with IAV PR8 at 100 PFU from day 0 to day 6. The average body weight of infected mice started to fall at day 3 postinfection and an approximately 26 % loss relative to the original weight was observed on day 6, but the average body weight of uninfected mice showed a continuous increase (Fig. 6A1). All animals survived during the experimental period except one infected animal, which died on day 6.

The viral NP levels in the lungs monitored by western immunoblotting showed that they started to increase at day 2 postinfection, reaching a peak at day 3 and then gradually decreasing (Fig. 6A2). Progressive and marked downregulation of β-catenin was noted during the infection period from day 2 to day 6 (Fig. 6B and C). This was coupled with simultaneous downregulation of phosphor-GSK-3β (Ser 9) (inactive form) expression in the lungs, and marked downregulation began at day 1 postinfection and persisted until day 6 postinfection. In contrast to these changes, total GSK-3β expression was steady until day 4 postinfection and was significantly upregulated at day 6. A mild and continuous decrease in the expression of VE-cadherin was detected until day 3 post-expression, followed by a marked decrease in expression from day 4 to day 6 postinfection. Changes in these expression levels were observed in the lungs at day 6 postinfection, the starting point of an obvious multi-organ failure phase with vascular hyperpermeability [15]. These *in vivo* changes in lung tissue added support to the *in vitro* findings of increased hyperpermeability after infection of HUVECs with IAV PR8.

## Discussion

The present study resulted in several new findings: (i) IAV PR8 infection markedly decreased the level of a regulatory component of the VE-cadherin cell adhesion complex, β-catenin, in association with enhanced permeability of human vascular endothelial cells. (ii) The decrease in β-catenin protein levels in the cells was the result of degradation by activation of GSK-3β, and the degradation was inhibited by lactacystin, a proteasome inhibitor. (iii) IAV infection-induced β-catenin degradation was suppressed in HUVECs by GSK-3β knockdown and restoration of cellular barrier function by transfection with β-catenin. (iv) There was marked downregulation of adherens junctional protein β-catenin and upregulation of dephosphorylated GSK-3β (active GSK-3β) in the lungs of mice infected with IAV PR8.

Until recently, anti-influenza agents that inhibit viral replication have represented the best treatment option. However, MOF appears just after influenza virus peak proliferation with the initiation of host immune responses and development of metabolic disorders [11, 15], and thus the use of antiviral neuraminidase inhibitors is not suitable for the treatment of MOF after viral proliferation. MOF induced by severe IAV infection is the final outcome of circulatory failure, hypoxemia, and vascular hyperpermeability of endothelial cells through the "influenza–cytokine–trypsin and matrix metalloprotease-9" cycle [8, 11], with disruption of vascular junctions. In a series of studies, we reported previously that upregulation of trypsin in brain vascular endothelial cells by pro-inflammatory cytokines after IAV infection plays a pivotal role in the destruction of tight junctions in the BBB through an increase in $[Ca^{2+}]_i$ and loss of ZO-1 via proteinase-activated receptor-2 signaling [8, 17].

Adherens junction, another major type of junction in the vascular endothelium, plays important roles in contact inhibition of endothelial cell growth and paracellular permeability to circulating leukocytes and solutes. Adherens junctions are ubiquitously distributed, and endothelial cells

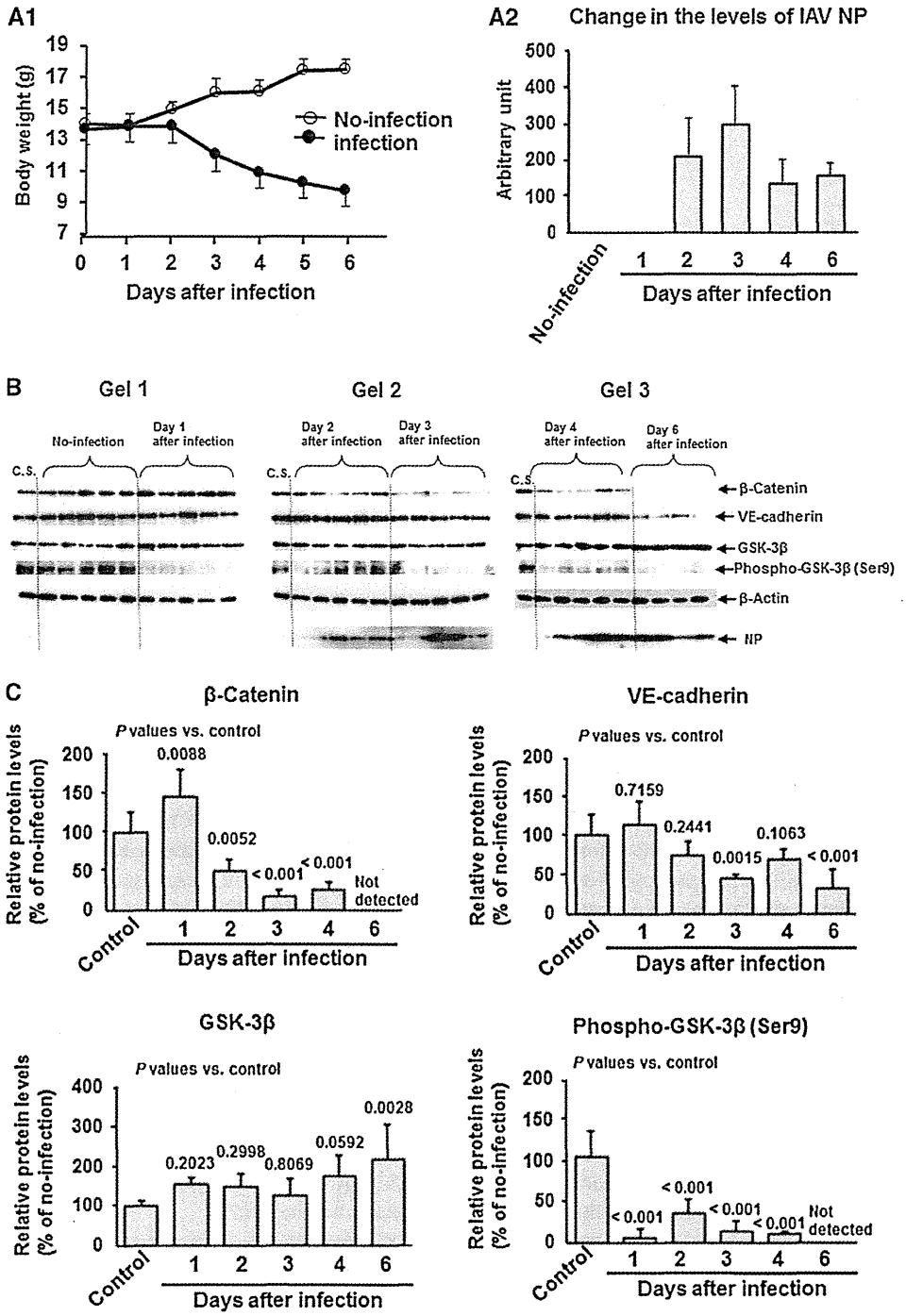


**Fig. 6** β-Catenin suppression and GSK-3β activation in lungs of IAV-infected mice. A1, change in body weight of infected and uninfected mice (five mice in each group). A2, change in viral NP levels in the lungs monitored by western immunoblotting (B). One infected animal died on day 6 postinfection. The values represent the mean ± SD of five or four mice. B and C, Data represent the expression levels (B) and relative quantified data (C) of β-catenin, VE-cadherin, GSK-3β, and phospho-GSK-3β (Ser9) in lung extracts (20 μg protein/lane) of control (no-infection) and IAV-infected mice from day 1 to day 6 postinfection. C.S., calibration standard (mixture of uninfected sample except for NP analysis) to normalize the intensity of protein bands in different gels. As the C.S. for NP, a sample from one animal after infection for 4 days was used. β-Actin was used as an internal control. Data are representative of three separate experiments. Multiple comparison (Dunnett test) after ANOVA were used for statistical analysis. *P*-values are relative to the control (no infection)

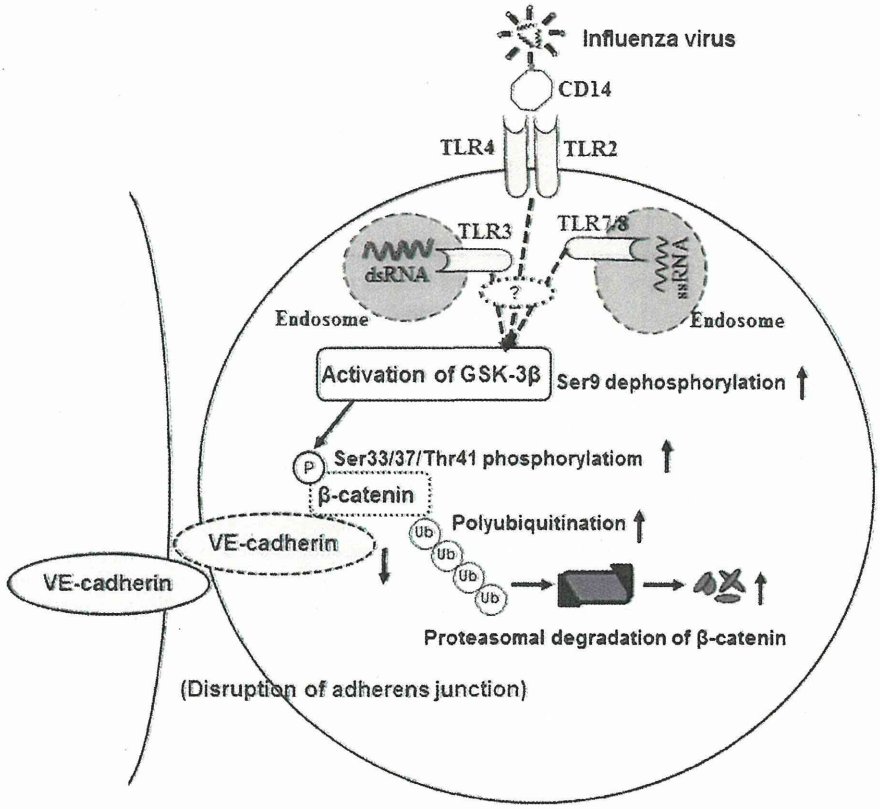


**Fig. 7** Diagram illustrating the proposed mechanism of disruption of the adherens junctional complexes of vascular endothelial cells after severe IAV infection. Infection of vascular endothelial cells with IAV decreases β-catenin in the VE-cadherin-β-catenin adhesive complex by activation of GSK-3β and the phosphorylation-dependent ubiquitin-proteasome degradation pathway. TLR, Toll-like receptor; dsDNA, double-stranded DNA; ssRNA, single-stranded RNA. The question mark indicates that signal transductions between TLRs and GSK-3β are unidentified

in all types of blood vessels express VE-cadherin. The cytoplasmic tail of VE-cadherin binds β-catenin and plakoglobin at the carboxy-terminal region, both of which link α-catenin and anchor the complex to the actin cytoskeleton [18]. The first of these, β-catenin is a major regulatory component of the VE-cadherin-β-catenin adhesive complex, and its level is tightly regulated by GSK-3β, followed by the phosphorylation-dependent ubiquitin-proteasome degradation pathway in a manner similar to the phosphorylation-dependent degradation of IκB [23].

As an extension to our previous studies on the mechanisms of vascular hyperpermeability in MOF caused by severe IAV infection, we studied the mechanisms of destruction of the VE-cadherin-β-catenin adhesive complex and vascular hyperpermeability after IAV infection in human endothelial cells, both *in vitro* and *in vivo*. Our results showed marked β-catenin degradation by proteasomes and a significant decrease in phosphorylated GSK-3β (Ser9) expression in HUVECs after IAV infection (Figs. 1, 3 and 6). The findings of downregulation of β-catenin after IAV infection through the activation of GSK-3β followed by the phosphorylation-dependent ubiquitin-proteasome degradation pathway were supported by the experiments of GSK-3β gene silencing. GSK-3β-gene-silenced HUVECs showed almost complete protection against β-catenin downregulation in cells infected with IAV (Fig. 4), and β-catenin degradation was inhibited by lactacystin (Fig. 2). In addition, expression of recombinant β-catenin in HUVECs almost completely restored monolayer hyperpermeability induced by IAV infection. These results indicate that the level of β-catenin in the VE-cadherin-β-catenin adhesive complex is important for regulation of vascular permeability and that the β-catenin level is regulated by the GSK-3β-mediated β-catenin degradation pathway. The findings with IAV-infected HUVECs support previous studies on β-catenin degradation in the absence of Wingless/Wnt signaling pathway via GSK-3β-mediated β-catenin phosphorylation and the phosphorylation-dependent ubiquitin-proteasome degradation pathway in various mammalian cells [23].

The mitochondria-mediated caspase activation pathway is a major apoptotic pathway characterized by mitochondrial outer membrane permeabilization [24], and degradation of β-catenin by caspase-3 in the signaling pathway of apoptosis is another major contributing factor to tissue and cell damage, including hyperpermeability of endothelial cells [25–28]. We reported previously that IAV infection induces hyperpermeability associated with mitochondrial dysregulation, calcium mobilization, and loss of ZO-1 via protease-activated receptor in HUVECs [8] and apoptosis via mitochondrial membrane depolarization in cardiomyoblasts [9]. Upregulated TNF-α also induces mitochondrial

dysregulation through increasing mitochondrial $O_2^-$ production and depleting ATP synthesis, decreasing oxygen consumption [10, 29], and increasing $[Ca^{2+}]_i$ [30].

GSK-3β is a serine/threonine protein kinase that has been shown recently to play a key role during the inflammatory response induced by various pathogenic bacteria, such as *Francisella tularensis*, the causative agent of highly virulent tularemia [31], *Burkholderia pseudomallei* [32] and group A streptococcus [33]. Bacterial lipopolysaccharides and lipid A are recognized by the Toll-like receptor (TLR)-2 on the cellular membrane and regulate GSK-3β activity via a phosphoinositide 3-kinase-Akt-dependent pathway [31]. In the present study, we found GSK-3β activation-mediated β-catenin degradation and monolayer hyperpermeability in IAV-infected HUVECs, and we propose a mechanism for the disruption of the adherens junctional complexes of vascular endothelial cells after severe IAV infection (Fig. 7). Since TLR2 and TLR4 bind to viral structural protein with CD14 [34], TLR7/8 binds to ssRNA and TLR3 binds to dsRNA [17], further studies on IAV-induced signal transduction from TLRs to GSK-3β activation are needed. In addition, there is also a need to design new therapeutic agents that can upregulate β-catenin and inhibit GSK-3β in vascular endothelial cells.

In summary, our results show that infection of HUVECs with IAV PR8 markedly decreases β-catenin levels in the VE-cadherin-β-catenin adhesive complex of HUVECs, together with hyperpermeability of HUVEC monolayers. The level of β-catenin in the adhesive complex is tightly regulated by activation of GSK-3β and the phosphorylation-dependent ubiquitin-proteasome degradation pathway. Destruction of the VE-cadherin-β-catenin adhesive complex could be one of the main pathomechanisms of MOF after severe IAV infection.

**Acknowledgments** The authors thank Dr. Junji Chida for stimulating discussion and comments. This research was funded in part by Grant-in-Aid 24249059 from the Ministry of Education, Culture, Sports, Science, and Technology of Japan and by a Health and Labor Sciences Research Grant (grant no. 12103307) from the Ministry of Health, Labor and Welfare of Japan.



## References

1. Lipatov MS, Govorkova EA, Webby RJ, Ozaki H, Peiris M et al (2004) Influenza: emergence and control. J Virol 78:8951–8959. doi:10.1128/JVI.78.17.8951-8959.2004
2. Kim HW, Brandt CD, Arrobio JO, Murphy B, Chanock RM et al (1979) Influenza A and B virus infection in infants and young children during the years 1957-1976. Am J Epidemiol 109:464–479
3. Chowell G, Echevarria-Zuno S, Viboud C, Simonsen L, Miller MA et al (2012) Epidemiological characteristics and underlying risk factors for mortality during the autumn 2009 pandemic wave in Mexico. PLoS One 7(7):e41069. doi:10.1371/journal.pone.0041069
4. Perkins LE, Swayne DE (2001) Pathobiology of A/chicken/Hong Kong/220/97 (H5N1) avian influenza virus in seven gallinaceous species. Vet Pathol 38:149–164. doi:10.1354/vp.38-2-149
5. Delorme L, Middleton PL (1979) Influenza A virus associated with acute encephalopathy. Am J Dis Child 133:822–824. doi:10.1001/archpedi.1979.02130080062011
6. Yao D, Mizuguchi H, Yamaguchi M, Yamada H, Chida J et al (2008) Thermal instability of compound variants of carnitine palmitoyltransferase II and impaired mitochondrial fuel utilization in influenza-associated encephalopathy. Hum Mutat 29:718–727. doi:10.1002/humu.20717
7. Yao M, Yao D, Yamaguchi M, Chida J, Yao D et al (2011) Bezafibrate upregulates carnitine palmitoyltransferase II expression and promotes mitochondrial energy crisis dissipation in fibroblasts of patients with influenza-associated encephalopathy. Mol Genet Metab 104:265–272. doi:10.1016/j.ymgme.2011.07.009
8. Wang S, Le TQ, Kurihara N, Chida J, Cisse Y et al (2010) Influenza virus–cytokine–protease cycle in the pathogenesis of vascular hyperpermeability in severe influenza. J Infect Dis 202:991–1001. doi:10.1086/656044
9. Pan HY, Yamada H, Chida J, Wang S, Yano M et al (2011) Upregulation of ectopic trypsins in the myocardium by influenza A virus infection triggers acute myocarditis. Cardiovasc Res 58:19–28. doi:10.1093/cvr/cvq358
10. Spraque AH, Khalil RA (2009) Inflammatory cytokines in vascular dysfunction and vascular disease. Biochem Pharmacol 78:539–552. doi:10.1016/j.bcp.2009.04.029
11. Yamane K, Indalao IL, Chida J, Yamamoto Y, Hanawa M et al (2014) Diisopropylamine dichloroacetate, a novel pyruvate dehydrogenase kinase 4 inhibitor, as a potential therapeutic agent for metabolic disorders and multiorgan failure in severe influenza. PLoS One 9(5):e98032. doi:10.1371/journal.pone.0098032
12. Le TQ, Kawachi M, Yamada H, Shiota M, Okumura Y et al (2006) Identification of trypsin I as a candidate for influenza A virus and Sendai virus envelope glycoprotein processing protease in rat brain. Biol Chem 387:467–475. doi:10.1515/BC.2006.062
13. Klenk HD, Rott R, Orlich M, Blödom J (1975) Activation of influenza A viruses by trypsin treatment. Virology 68:426–439. doi:10.1016/0042-6822(75)90284-6
14. Kido H, Okumura Y, Yamada H, Le TQ, Yano M (2007) Proteases essential for human influenza virus entry into cells and their inhibitors as potential therapeutic agents. Curr Pharm Des 13:405–414. doi:10.2174/138161207780162971
15. Kido H, Okumura Y, Takahashi E, Pan HY, Wang S et al (2012) Role of host cellular proteases in the pathogenesis of influenza and influenza-induced multiple organ failure. Biochim Biophys Acta 1824:186–194. doi:10.1016/j.bbapap.2011.07.001
16. Niu QX, Chen HQ, Chen ZY, Fu YL, Lin JL et al (2008) Induction of inflammatory cytokine release from human umbilical vein endothelial cells by agonists of proteinase-activated receptor-2. Clin Exp Pharmacol Physiol 35:89–96. doi:10.1111/j.1440-1681.2007.04755.x
17. Pan HY, Yano M, Kido H (2011) Effects of inhibitors of Toll-like receptors, protease-activated receptor-2 signalings and trypsin on influenza A virus replication and upregulation of cellular factors in cardiomyocytes. J Med Invest 58:19–28. doi:10.2152/jmi.58.19
18. Bazzono G, Dejana E (2004) Endothelial cell-to-cell junctions: molecular organization and role in vascular homeostasis. Physiol Rev 84:869–901